Journal of Theoretical Biology 408 (2016) 1–12

Contents lists available at ScienceDirect

Journal of Theoretical Biology

journal homepage: www.elsevier.com/locate/yjtbi

A multiscale model of placental oxygen exchange: The effect of villous tree structure on exchange efficiency

Mabelle Lin [a], Benjamin Mauroy [b], Joanna L. James [c], Merryn H. Tawhai [a], Alys R. Clark [a,*]

[a] Auckland Bioengineering Institute, The University of Auckland, Auckland, New Zealand
[b] Laboratoire J. A. Dieudonné - UMR CNRS 7351, Université de Nice-Sophia Antipolis, Nice, France
[c] Department of Obstetrics and Gynaecology, Faculty of Medical and Health Sciences, University of Auckland, New Zealand

HIGHLIGHTS

- A new oxygen exchange model incorporating a villous tree structure is proposed.
- Key associations between oxygen exchange and villous tree structure are identified.
- Villous tree structure influences intervillous blood flow and oxygen uptake capacity.

GRAPHICAL ABSTRACT

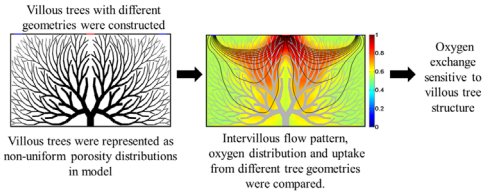

ARTICLE INFO

Article history:
Received 29 January 2016
Received in revised form
29 June 2016
Accepted 30 June 2016
Available online 1 July 2016

Keywords:
Placenta
Placental structure
Intervillous blood flow
Gas exchange
Computational model

ABSTRACT

The placenta is critical to fetal health during pregnancy as it supplies oxygen and nutrients to maintain life. It has a complex structure, and alterations to this structure across spatial scales are associated with several pregnancy complications, including intrauterine growth restriction (IUGR). The relationship between placental structure and its efficiency as an oxygen exchanger is not well understood in normal or pathological pregnancies. Here we present a computational framework that predicts oxygen transport in the placenta which accounts for blood and oxygen transport in the space around a placental functional unit (the villous tree). The model includes the well-defined branching structure of the largest villous tree branches, as well as a smoothed representation of the small terminal villi that comprise the placenta's gas exchange interfaces. The model demonstrates that oxygen exchange is sensitive to villous tree geometry, including the villous branch length and volume, which are seen to change in IUGR. This is because, to be an efficient exchanger, the architecture of the villous tree must provide a balance between maximising the surface area available for exchange, and the opposing condition of allowing sufficient maternal blood flow to penetrate into the space surrounding the tree. The model also predicts an optimum oxygen exchange when the branch angle is 24 °, as villous branches and TBs are spread out sufficiently to channel maternal blood flow deep into the placental tissue for oxygen exchange without being shunted directly into the DVs. Without concurrent change in the branch length and angles, the model predicts that the number of branching generations has a small influence on oxygen exchange. The modelling framework is presented in 2D for simplicity but is extendible to 3D or to incorporate the high-resolution imaging data that is currently evolving to better quantify placental structure.

1. Introduction

The human placenta is crucial for the survival and health of a fetus. It is the only exchange interface that provides the fetus with nutrients and oxygen during pregnancy. Numerous pregnancy complications such as preeclampsia and intrauterine growth

* Corresponding author.
E-mail addresses: mlin865@aucklanduni.ac.nz (M. Lin), benjamin.mauroy@unice.fr (B. Mauroy), j.james@auckland.ac.nz (J.L. James), m.tawhai@auckland.ac.nz (M.H. Tawhai), alys.clark@auckland.ac.nz (A.R. Clark).

http://dx.doi.org/10.1016/j.jtbi.2016.06.037
0022-5193/

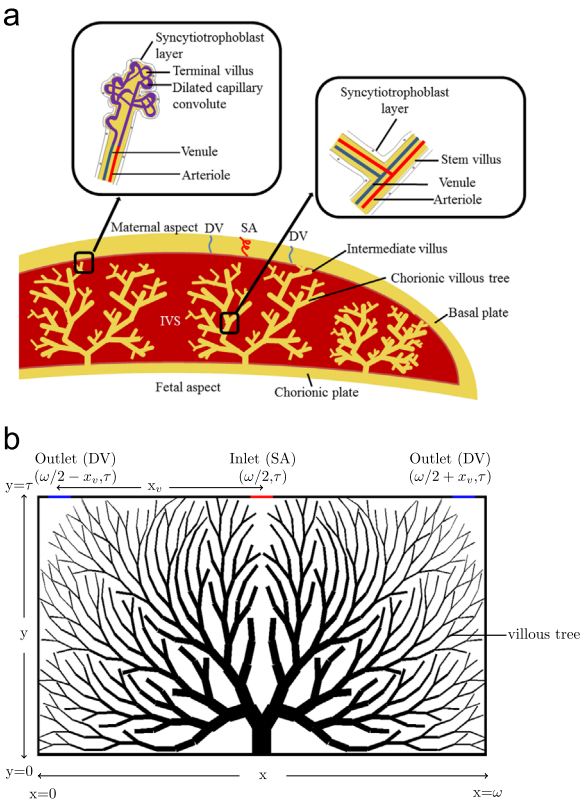

Fig. 1. (a) A schematic diagram of the human placenta at term. The placenta contains numerous chorionic villous trees which stem from the chorionic plate of the placenta into the intervillous space (IVS). Maternal blood enters the IVS from the uterine spiral arteries (SA), percolates through the IVS around the villi before draining through the decidual veins (DV). The fetal circulation resides within the villous trees, and generally runs along the branches in stem and intermediate villi before reaching a dilated and convoluted capillary structure in the terminal villi. Oxygen, nutrients and wastes are exchanged between the maternal circulation and the fetal circulation across the syncytiotrophoblast layer. (b) Model representation of a placental subunit represented by a 2D domain of thickness τ and width ω. Each subunit contains a representative villous tree generated from realistic morphometric parameters fed by a central SA and drained by two DVs. The most distal branches of the villous tree shown are termed intermediate villi, and these villi are assumed to supply 'terminal tissue blocks'.

restriction (IUGR) have been associated with placental malfunction (Regnault et al., 2002). While morphological abnormalities have been identified in pathological placentas (Mayhew et al., 2003; Krebs et al., 1996; Egbor et al., 2006), it is not fully understood how these translate to abnormalities in placental function.

Fig. 1a shows a schematic of placental structure. It contains numerous branching structures known as chorionic villous trees, each of which comprises a network of fetal blood vessels. The largest branches of the villous trees (termed stem and intermediate villi) contain one or more arteriole or venule, and these blood vessels branch along with the villous tree structure. In the smallest villi (terminal villi), dilated capillary convolutes reside close to the villus surface. This surface is covered by a single multinucleated cell layer called the syncytiotrophoblast. The proximity of blood vessels to the surface of the villous tree provides an exchange interface to extract oxygen and nutrients from maternal blood that flows through the intervillous space (IVS) surrounding the villous trees, while keeping the fetal circulation separate from the maternal circulation.

Morphological abnormalities associated with pathology include reduced volume and surface area of terminal villi (Mayhew et al., 2003; Egbor et al., 2006), decreased villus length (Mayhew et al., 2003; Egbor et al., 2006), increased trophoblast epithelium thickness (Mayhew et al., 2003) and abnormally sparse capillary networks (Krebs et al., 1996; Kingdom and Kaufmann, 1997). However, the relationship between these villus abnormalities and the functionality of the placenta is not well defined. Most animal models of the placenta are difficult to extrapolate to human because the placenta displays a wide structural diversity between species (Benirschke et al., 2006). For ethical reasons, it is also impossible to perform invasive experiments or collect measurements directly from the human fetus or placenta during the course of pregnancy. Therefore, although the placenta can be imaged *in vivo* using ultrasound (Pretorius et al., 1998) and magnetic resonance imaging (Sørensen et al., 2013), the resolution of these techniques is currently not sufficient to relate the *in vivo* orientation of villous trees to incoming flow from the maternal spiral arteries, or to extrapolate imaging data to the functionality of the placenta.

In view of the difficulties in directly measuring placental function, there is a need to establish tools to investigate how observed pathologies in villous tree structure influence the functionality of the human placenta. Computational models are emerging as a useful tool to address this problem. Early models of oxygen delivery and uptake within the placenta placed particular emphasis on modelling the exchange of oxygen and carbon dioxide between the maternal and fetal bloodstreams at terminal villi (Hill et al., 1972, 1973). These models include detail on gas uptake dynamics but neglect the spatial flow characteristics of the maternal circulation and its resultant impact on gaseous exchange.

Later models considered maternal flow in the IVS as a porous medium (Erian et al., 1977; Schmid-Schobein, 1988). Erian et al. (1977) modelled the intervillous space in 2D, and assuming that the villous tree is significantly deformed by maternal flow, a flow-dependent tissue permeability was included into their model. Chernyavsky et al. (2010) combined a 3D axisymmetric porous medium approach and first order solute uptake kinetics by a homogenised villous tree (uniform porosity throughout). These porous medium models have predicted 'short-circuiting' of maternal blood flow from maternal spiral arteries to decidual veins when there are highly permeable regions in the vicinity of these arteries and veins (Erian et al., 1977), and when arteries and veins are in close vicinity (Chernyavsky et al., 2010). In this case, there is an effective shunt as oxygenated blood does not circulate around the villous tree before leaving the IVS. This type of model also suggested that greater distances between spiral arteries and decidual veins facilitate nutrient delivery in the IVS. Chernyavsky et al. (2011) employed a simple model of flow and diffusion around distributed point sinks and statistical analysis of 2D placental sections to estimate the potential error incurred in homogenisation of IVS tissue to uniform or slowly varying area fractions. They showed that the accuracy of homogenisation approaches depended on flow characteristics (Peclet and Damkohler numbers), as well as the relative size of intervillous distances and typical pathlengths from spiral arteries to decidual veins. Recently, Lecarpentier et al. (2016) used the Navier-Stokes equations to model blood flow between 'rigid' tissue obstacles in a 2D representation of the IVS. This approach includes significant geometric detail but is computationally expensive so does not lend itself to large scale simulations of blood flow and/or nutrient transport in the whole placenta. Serov et al. (2015), Serov et al. (2015) took a very different approach to simulating placental oxygen exchange, introducing a stream-tube model of oxygen exchange in a placental subunit. This model predicted optimal placental efficiency at tissue volume fraction that corresponds well to those found in normal placentas. Comprehensive reviews of placental exchange models can be found in earlier publications (Chernyavsky et al., 2010; Serov et al., 2015).

Existing placental exchange models are simplified geometrically, either by assuming that the villous tissue is homogenous

Please cite this article as: Lin, M., et al., A multiscale model of placental oxygen exchange: The effect of villous tree structure on exchange efficiency. J. Theor. Biol. (2016), http://dx.doi.org/10.1016/j.jtbi.2016.06.037

with uniform uptake potential everywhere apart from at a central cavity (Chernyavsky et al., 2010), or assuming that maternal blood flow streamlines follow villous branches with oxygen uptake occurring across the surface of these branches which extends uniformly along the branch length from the central cavity to the decidual vein (Serov et al., 2015). These geometric simplifications allow analytical (rapid) solution of models to predict function, and can be parameterised by assessment of histological slides showing the size and distribution of villous trees. These models have suggested different estimates of optimal villous tissue density for placental efficiency, with estimates from the stream-tube model comparing well to stereological data (Serov et al., 2015). However, these models do not explicitly account for the branching architecture of the villous tree, which has been suggested to improve the accuracy of model predictions (Serov et al., 2015). A recent multiscale model of the placental vasculature (Clark et al., 2015) suggested that vascular branching may influence placental efficiency, but did not attempt to model oxygen exchange.

Current models of oxygen exchange in the placenta assume a uniform oxygen exchange potential at any point within the villous tree structure; for example, there is no distinction between terminal and stem villi in terms of exchange barrier thickness. The harmonic mean barrier thickness between maternal and fetal blood varies through the placenta with the thinnest barriers (and most mature terminal villi) residing peripherally in the placental subunit (Critchley and Burton, 1987; Hempstock et al., 2003). It has been theorised that peripheral villi are more effective gas exchangers than central ones, as they reside in a lower oxygen environment than central villi. A central to peripheral gradient in oxygen concentration has been confirmed in primate placental subunits (Ramsey et al., 1963; Richart et al., 1964), and is consistent with hypothesised blood flow distributions (Wigglesworth, 1969), and has been visualised in humans using BOLD MRI (Sørensen et al., 2013)). To date computational models of placental oxygen exchange have not been able to account for these structural and functional inhomogeneities.

Here, we present a computational framework to model oxygen transport in a placental subunit, which aims to bridge the gap between detailed geometric models (Clark et al., 2015; Lecarpentier et al., 2016) and highly smoothed homogeneous models (Chernyavsky et al., 2011, 2010; Serov et al., 2015, 2015), providing a picture of how the architecture of the placental villi influences oxygen delivery. Like Erian's model, this modelling framework is presented in 2D for simplicity but is extendible to 3D. The model is parameterised here using morphological data and can be incorporated with imaging data. Our model predicts how maternal blood flow in a human placental subunit is influenced by a non-uniform porosity distribution over the villous structure, and whether regional variations in oxygen uptake capacity influence placental efficiency. Our aim is to examine the influences of villous tree geometry on maternal blood flow patterns, distribution of oxygen in the IVS and fetal oxygen uptake rate.

2. Materials and methods

Our model incorporates key aspects of placental structure to simulate the distribution and uptake of oxygen within a functional unit surrounding a representative villous tree (a placentome, Fig. 1b). A schematic of model components and key outputs is given in Fig. 2, and each component is described below. The model is solved using a custom written Matlab®(The Mathworks Inc., version 2012b) finite element code.

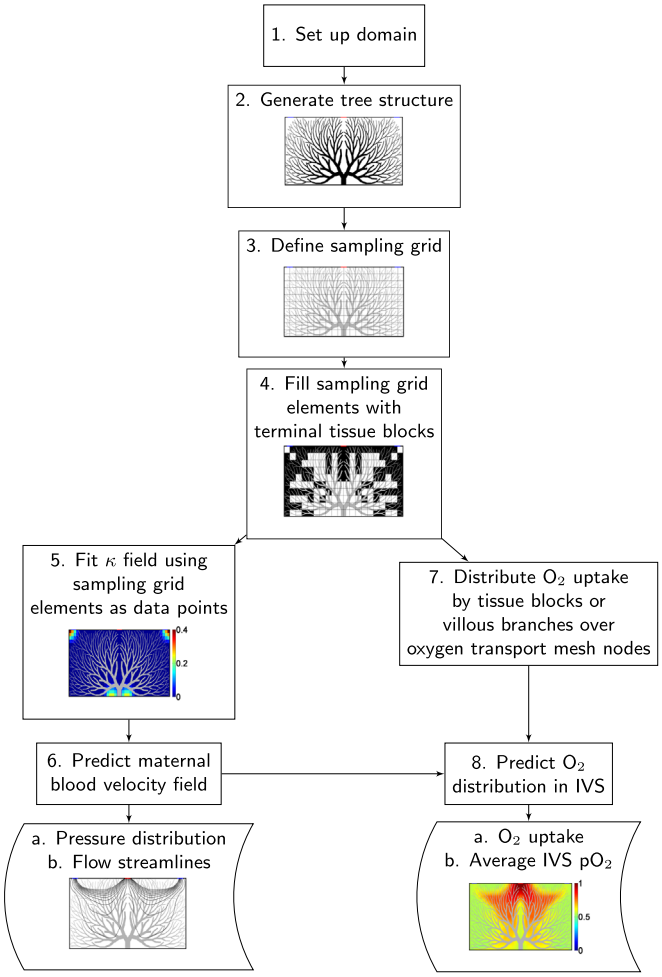

Fig. 2. Schematic showing how model components fit together for generation of model solution.

2.1. Model geometry

Following previous studies (Erian et al., 1977), we assumed a 2D rectangular domain to represent a placental subunit (Fig. 1b), which assumes that the placenta is of uniform thickness in the region of a villous tree. The domain has thickness τ, which spans the distance between the basal plate and the chorionic plate (Fig. 1a), and width ω. Due to the lack of quantitative assessment of the distribution of maternal vasculature with respect to the villous trees, we followed previous studies (Erian et al., 1977; Chernyavsky et al., 2010; Serov et al., 2015, 2015) and assumed that the placental subunit is fed by one central spiral artery (SA) and drained by two decidual veins (DVs), with one DV at a fixed distance (x_v) on each side of the SA. The SA and DVs were assumed to have a fixed diameter d.

2.1.1. Representation of the villous tree

The branching component of the villous tree has been described in several studies (Benirschke et al., 2006, Leiser 1991, Castellucci et al., 1990). Referring to Fig. 1a, the villous branches at the interface between the chorionic plate and the villous trees are termed stem villi and have a diameter of up to 1.7 mm (Leiser et al., 1991). They divide up to 15 branching generations to numerous intermediate villi (diameter around 60 μm (Leiser et al., 1991)) to supply the terminal villi. The terminal villi are convoluted structures in which fetal capillaries come in close proximity to maternal blood (Benirschke et al., 2006). The villus

Please cite this article as: Lin, M., et al., A multiscale model of placental oxygen exchange: The effect of villous tree structure on exchange efficiency. J. Theor. Biol. (2016), http://dx.doi.org/10.1016/j.jtbi.2016.06.037

Table 1
Model parameters, including chosen nominal value and literature range at term.

Parameter	Description	Nominal value	Range	References
Model Geometry				
τ	Domain thickness (mm)	20	20-45	Benirschke et al. (2006), Chernyavsky et al. (2010), Boyd and Hamilton (1970), Johannigmann et al. (1972)
ω	Domain width (mm)	40	10-40	Benirschke et al. (2006), Chernyavsky et al. (2010)
x_v	Distance between SA and DV (mm)	18	unknown	–
d	Diameter of SA and DVs (mm)	2	2-3	Wigglesworth (1969), Harris and Ramsey (1966)
n_b	Number of branching generations	15	up to 15	Leiser et al. (1991)
l_s	Stem length (mm)	2	2	Leiser et al. (1991)
d_s	Stem diameter (mm)	1.7	1.7	Leiser et al. (1991)
l_d/l_p	Daughter/parent branch length ratio	0.975	1	Leiser et al. (1991)
d_d/d_p	Daughter/parent branch diameter ratio	0.8	~0.8	Leiser et al. (1991)
θ_b	Branch angle	18°	40°-70° (terminal branches)	Haeussner et al. (2014)
ϕ_{TV}	Terminal villus area fraction	0.4	0.28-0.4	Mayhew et al. (2003), Egbor et al. (2006)
d_{TV}	Terminal villus diameter (mm)	0.05	0.03-0.06	Egbor et al. (2006), Leiser et al. (1991)
Blood flow model				
μ	Blood viscosity (Pa.s)	4×10^{-3}	4×10^{-3}	Chernyavsky et al. (2010)
P_{in}	Inlet blood pressure (mmHg)	18.8	9-12	Chernyavsky et al. (2010), Burton et al. (2009)
P_{out}	Outlet blood pressure (mmHg)	1.10×10^{-3}	3-5	Chernyavsky et al. (2010), Burton et al. (2009)
κ_{empty}	Maximum hydraulic conductivity (mm^2)	0.52	∞	–
Oxygen transport model				
D	Diffusivity of oxygen in blood (cm^2/s)	1.62×10^{-5}	1.62×10^{-5}	Goldstick et al. (1976)
C_f	Oxygen concentration in fetal blood(ml/ml)	8.72×10^{-2}	8.72×10^{-2}-2.08×10^{-1}	Acharya and Sitras (2009)
α	Oxygen uptake constant (s^{-1})	0.38	unknown	–
C_{in}	Oxygen concentration entering through SA (ml/ml)	1.64×10^{-1}	1.63×10^{-1}-1.66×10^{-1}	Supplementary Material (Section C), Schaaps et al. (2005)

structures to the level of the intermediate villi can be considered as distinct branches for modelling purposes, but beyond that level the villus structures become too numerous to be included individually in a model, with a branching structure that is not well described (Clark et al., 2015).

Branching component: A rule-based algorithm, described in detail in the Supplementary Material (Section A) was used to generate a villous tree structure to the level of the intermediate villi. The algorithm is controlled by the following parameters: the number of branching generations (n_b), stem length (l_s), stem diameter (d_s), daughter to parent branch length ratio (l_d/l_p), daughter to parent branch diameter ratio (d_d/d_p) and branch angle between the daughter branch and its parent branch (θ_b). These parameters, together with the condition that there must be sufficient space for a branch to grow within the domain boundary, define a bifurcating tree as shown in Fig. 2, step 2. Physiological ranges for these parameters at term are given in Table 1. The most distal villi shown represent the intermediate villi. Using the parameters defined in Table 1, a villous tree comprised of 15 branching generations with 202 terminals was generated.

Beyond the intermediate villi: The convoluted terminal villi beyond the intermediate villi were modelled as homogenised 'terminal tissue blocks' (TBs), with villous tissue density as measured in stereological studies investigating the morphological properties of terminal villous tissue (Mayhew et al., 2003; Egbor et al., 2006). To do this, a sampling grid was superimposed over the tree structure (Fig. 2, step 3), and each element of the sampling grid containing intermediate villi was assigned to be a TB with a villous tissue area fraction (ϕ_{TV}), and an average villus diameter (d_{TV}) as given in Table 1 (Fig. 2, step 4). The size of elements in the sampling grid (and so the size of each TB) was estimated to be representative of the space occupied by terminal villous tissue arising from each intermediate villus. The cumulative length of a terminal convolute branching from an intermediate villus has been estimated to be l_{TV}=3 mm, and there are approximately n_{TV} =8-10 terminal convolutes branching from a mature intermediate villus (Leiser et al., 1991). Therefore, the area occupied by terminal villi arising from a single intermediate villus can be estimated by $l_{TV} n_{TV} d_{TV}$. The appropriate sampling grid size is then

$$\frac{l_{TV} n_{TV} d_{TV}}{\phi_{TV}}. \quad (1)$$

Based on the parameter ranges in Table 1, an appropriate sampling grid size at term is 2 mm × 2 mm.

2.2. Maternal blood flow

Governing equations: To explicitly model the fluid dynamics of blood in the IVS between the numerous generations of villi would be computationally impractical even in a placental subunit. Therefore, we assume that the IVS can be represented as a porous medium (Erian et al., 1977; Schmid-Schobein, 1988; Chernyavsky et al., 2010). However, we defined hydraulic conductivity ($\kappa = \kappa(x, y)$) as a spatially varying quantity calculated from the generated tree and tissue structure (Fig. 2, step 5). Maternal blood

Please cite this article as: Lin, M., et al., A multiscale model of placental oxygen exchange: The effect of villous tree structure on exchange efficiency. J. Theor. Biol. (2016), http://dx.doi.org/10.1016/j.jtbi.2016.06.037

flow was therefore modelled using Darcy's law:

$$\nabla \cdot \mathbf{U} = 0, \tag{2a}$$

$$\mathbf{U} = -\frac{\kappa}{\mu}\nabla P, \tag{2b}$$

where $\mathbf{U}$ is the average blood velocity in the IVS, μ is the viscosity of maternal blood, and ∇P is the local maternal blood pressure gradient.

Finite element mesh and solution procedure: The sampling grid was refined once to obtain a finite element mesh with element size of 1 mm × 1 mm (the maternal flow mesh). The mesh was then triangulated to obtain a mixed finite element mesh and the lowest Raviart-Thomas mixed finite element method was implemented to solve Eq. (2) for the maternal blood velocity field (Bahriawati and Carstensen, 2005).

Boundary conditions: Pressure boundary conditions were prescribed at the inlet SA ($P = P_{in}$) and outlet DVs ($P = P_{out}$). P_{in} and P_{out} were fitted in the baseline case to obtain a flow velocity at the inlet element edge that matches literature estimates of volumetric flow from a single SA (Q_{in}). The two pressures were then held constant between simulations. Assuming a total maternal blood flow of 500-750 ml/min in a term placenta (Chernyavsky et al., 2010), and assuming 100 SAs (Lyall, 2005), a value for Q_{in} of 5 ml/min is calculated. The basal and chorionic plates act as barriers to flow in the IVS, so the y-component of velocity was set to zero at these boundaries ($U_y(x, 0) = U_y(x, \tau) = 0$ except at the inlet and outlets). At $x=0$ and $x = \omega$, the boundaries between placental subunits, a symmetry condition was applied ($U(0, y) = U(\omega, y)$).

Derivation of a hydraulic conductivity field: The hydraulic conductivity coefficient in Eq. (2b), was expressed using the Kozeny-Carman formula:

$$\kappa = \frac{d_{villi}^2}{180}\frac{(1-\phi)^3}{\phi^2}, \tag{3}$$

where d_{villi} is the average diameter of villi in the IVS and ϕ is the tissue density of villous tissue. Each element in the sampling grid was assigned a unique isotropic κ value, which represented the conductivity of tissue branches in that element or TB. The contribution to κ of the TBs is defined by ϕ_{TV} and d_{TV}. The contribution of discrete villous branches in each element was defined using a weighted average of the diameter of villi in the element and the area occupied by branches. The maximum value of κ in each element was prescribed a value of κ_{empty}. A smooth spatially varying field for κ (Fig. 2, step 5) was obtained for each element of the maternal flow mesh by sampling κ at each element of the sampling grid (Fig. 2, step 3) and averaging κ over all elements surrounding each node of the sampling grid. Smoothing was then implemented via a linear interpolation to determine κ at the midpoint of each maternal flow mesh element based on the generated nodal data, and the resultant value for κ was assigned to that element.

2.3. Oxygen transport and uptake

Governing equations: Oxygen concentration in the maternal blood within the IVS (C_m) was described by the advection-diffusion equation:

$$\frac{\partial C_m}{\partial t} + \mathbf{U}\cdot\nabla C_m = D\nabla^2 C_m - \alpha(C_m - C_f), \tag{4}$$

where t is time, $\mathbf{U}$ is the velocity field calculated from Eq. (2), D is the diffusivity of oxygen in maternal blood, C_f is the oxygen concentration in the fetal bloodstream and α is the oxygen uptake constant. Oxygen was assumed to be removed immediately by the fetal bloodstream upon uptake, so C_f is constant.

Finite element mesh and solution procedure: A finite element mesh comprised of bilinear elements was used to solve Eq. (4) (the oxygen transport mesh). The spatial resolution of this mesh is the same as the maternal flow mesh. Eq. (4) was solved using the Lagrange-Galerkin finite element method (Supplementary Material, Section B) (Croucher and O'Sullivan, 1998). This is a split operator approach in which, over each time step, the departure point of blood at each mesh node is calculated and C_m at that mesh node is initiated with the concentration at the blood's departure point at the start of the timestep. The updated oxygen concentration field is then used as an initial condition to calculate the new oxygen distribution resulting from diffusion using the finite element method. Typical timestep sizes to achieve temporal convergence were $5 \times 10^{-6} - 5 \times 10^{-3}$ s. The model was solved to the steady state.

Oxygen uptake by terminal villi: At the terminal villus level, oxygen uptake was assumed to occur over the whole region bound by the TB. Using the endpoint location of each intermediate villus feeding a TB, α is distributed to each of the nodes of the sampling grid element using a bilinear interpolation function. The resulting α distribution is sampled over the oxygen transport mesh when the model was solved.

Oxygen uptake by stem and intermediate villus branches: As the stem and intermediate villus branches were explicitly modelled, α was assigned at the start and end of every branch. For each villus, α was distributed between the nodes of the oxygen transport mesh element containing the villus. The α distribution for TBs and non-terminal villi were summed to obtain an overall α distribution for solution of Eq. (4) (Fig 2, step 7).

Boundary conditions: The oxygen concentration of the maternal blood entering the domain through the SA was assumed constant (C_{in}). At all other boundaries, a zero diffusive flux was imposed ($-D\nabla(C_m)\cdot\mathbf{n} = 0$, where $\mathbf{n}$ is the outward facing normal to the boundary). Oxygen is carried out of the DVs via the advective component of the solution.

2.4. Model outputs and parameterisation

Key model outputs are the flow and pressure distributions of maternal blood, the rate of oxygen uptake by the villous tree and the distribution of oxygen concentration in the IVS (Fig. 2). The rate of oxygen uptake by the villous tree was computed as the difference between the concentration flux at the inlet SA and the outlet DVs, while the average oxygen content in the IVS was calculated by dividing the sum of oxygen content at all finite element nodes in the 2D domain by the total number of finite element nodes. As in previous studies, the model was parameterised to the term placenta. Nominal model parameters and ranges from the literature are listed in Table 1.

The thickness (τ) and width (ω) of the domain were chosen following Chernyavsky et al. (2010). However, estimates for placental dimensions vary in the literature. *Ex vivo* and *in vivo* estimates of placental volume are quite consistent at term (de Paula et al., 2008; Boyd and Hamilton, 1970), although due to the loss of placental turgidity after delivery, placental thickness estimates vary between studies (Boyd and Hamilton, 1970; Johannigmann et al., 1972). For a given placental volume, the value of ω is then expected to vary with τ. Due to the lack of quantitative studies on DVs distribution over the basal plate, x_v was also chosen based on a previous model (Chernyavsky et al., 2010), where an optimum delivery of nutrients was predicted when DVs are located near the periphery of the placental subunit.

Estimation of the terminal villus density (ϕ_{TV}) varies between studies (Mayhew et al., 2003; Egbor et al., 2006). The tissue

Please cite this article as: Lin, M., et al., A multiscale model of placental oxygen exchange: The effect of villous tree structure on exchange efficiency. J. Theor. Biol. (2016), http://dx.doi.org/10.1016/j.jtbi.2016.06.037

density estimated by Egbor et al. (2006) was used as the nominal value as the study also provided morphometric data for a variety of pathological conditions, for comparison to the healthy case. The diameter of terminal villi (d_{TV}) is generally within the range of 0.03-0.06 mm (Egbor et al., 2006; Leiser et al., 1991) and hence, a mid-range value of 0.05 mm was assigned as the nominal value.

Hydraulic conductivity is infinite in an empty sampling grid element, but allowing such data points results in sharp fronts during field fitting which is cumbersome to deal with computationally. To overcome this, the maximum κ calculated from the sampling grid was scaled up by 10 times and set as the nominal value for κ_{empty}.

The oxygen content in fetal bloodstream (C_f) was derived from oxygen measurements in the umbilical artery immediately after delivery (Acharya and Sitras, 2009), while the oxygen content in the SA (C_{in}) was based on measurements in the uterine artery collected from pregnant women during their cesarean section (Schaaps et al., 2005). Conversion of partial pressure of oxygen to oxygen concentration is detailed in the Supplementary Material (Section C). The oxygen uptake constant (α) is predominantly defined by the diffusing capacity of the exchange barrier (Mayhew et al., 1984). Although the properties of the exchange barrier vary regionally in the placenta, a constant 0.38 s^{-1} was set throughout the subunit as the nominal case and subsequently varied to examine how regional variation in α affects oxygen uptake efficiency.

3. Results

3.1. Baseline case, consistency with previous studies

The model makes several predictions on the whole placentome scale that are directly comparable to previous experimental and modelling studies. These predictions are described briefly here, and are included in more detail in the Supplementary Material for completeness.

Function of a placental subunit: Table 2 shows model predictions of blood flow and oxygen exchange metrics in the placental subunit under baseline conditions (using nominal parameter values). Under these conditions, the model shows consistency with experimental data, except in the ratio of venous return pO_2 to that in the IVS. This ratio is different from the ratio recorded by Schaaps et al. (2005) for pO_2 in the uterine vein to the IVS. That study attributed higher measured pO_2 in the uterine vein to the vascular anastomoses in the myometrium and since such anastomoses were not incorporated in the current model, the ratio of pO_2 in venous return to IVS is expected to be different and should be less than 1.

Flow streamlines: In the baseline case, blood flow streamlines are consistent with previous model (Chernyavsky et al., 2010) and experimental (Wigglesworth, 1969) studies describing high flow and pressure near the SA inlets and a rapid dissipation of flow and pressure in regions comprising dense villous tissue, where blood percolates rather than streams. However, unlike the regular streamlines which conform to the hemispherical domain in earlier porous medium model due to the placement of DVs with respect to SA (Chernyavsky et al., 2010), the model generates irregular streamlines which have a tendency to pass through regions with higher hydraulic conductivity made up of non-terminal villous branches with sparse terminal tissue blocks (TBs) over areas with dense TBs, which is expected from a porous medium with spatially varying porosity.

Optimal villus density: Previous studies have assessed the relationship between villus density and oxygen exchange (Chernyavsky et al., 2010; Serov et al., 2015), while neglecting the branching component of the villous tree. Our model comprises two components of villus density, terminal villus density, ϕ_{TV}, and a contribution from the branching component of the tree. Our model peaks in oxygen uptake at $\phi_{TV} \approx 0.15$ (average density of all villi ≈0.24). This is consistent with previous porous medium model (Chernyavsky et al., 2010), in terms of optimal total villus density, but lower than the optimal villus density predicted by stream-tube model (Serov et al., 2015).

The effect of a central cavity: For consistency with previous models (Erian et al., 1977; Chernyavsky et al., 2010), the model was solved using an artificially applied 'central cavity', represented by a relatively villus-free region with a hydraulic conductivity of κ_{empty}, having the same length and width of a typical cavity. Detailed results are given in Supplementary Material (Section D.3), and predictions are consistent with previous studies (Chernyavsky et al., 2010) in that oxygen uptake is higher in the presence of a central cavity as blood is able to penetrate further and deeper into the IVS.

Table 2
Comparison of predicted blood flow and oxygen exchange metrics in a placental subunit simulated under baseline conditions with literature data.

Metric	Predicted value	Literature range	References
Oxygen uptake in subunit (ml/min)	0.36	0.18-0.63	Bonds et al. (1986)
Average pO_2 in IVS (mmHg)	33	23.3-33.9	Schaaps et al. (2005), Quilligan et al. (1960)
Ratio of pO_2 in venous return to IVS	0.90	1.48	Schaaps et al. (2005)

3.2. Parameter sensitivity

Table 3 shows sensitivity of predictions of oxygen consumption to model parameters. Referring to Table 1, the parameters α, κ_{empty} and x_v could not be estimated directly from the literature. The model is relatively insensitive to changes in α and κ_{empty}. However, as expected, the model is sensitive to x_v. Our model shows a decrease in oxygen uptake if DVs are situated closer to SAs, consistent with previous porous medium models (Chernyavsky et al., 2010). The predicted oxygen uptake rate is sensitive to the amount of oxygen brought into the placenta, via changes in Q_{in} (brought upon by altered P_{in} or SA diameter, d) or an altered C_{in}. Also, changes in C_f, which reflect changes in fetal metabolism, significantly influence predictions of oxygen consumption. Overall, geometrical parameters such as villous tissue density and the branching structure of the villous tree, which is the new feature introduced in this model, have the largest effect on model predictions of oxygen consumption. This is consistent with the concept of placental branching structure having a major influence on function. Each major structural contributor to predicted function is addressed below.

3.3. The branching structure of non-terminal villi

The structure of the branching component of the villous tree (the stem and intermediate villi) plays an important role in predicted oxygen consumption. In the model with baseline parameterisation, the villous branches act as both a barrier to blood flow (via their contribution to IVS conductivity) and as an oxygen exchange surface. In addition, the distribution of branches within the IVS influences whether the villous tree is 'space-filling': large empty spaces might be expected to allow free movement of maternal blood but could potentially reduce the number, and affect the distribution of terminal villi, which are the major sites for oxygen exchange, due to space constraint.

Please cite this article as: Lin, M., et al., A multiscale model of placental oxygen exchange: The effect of villous tree structure on exchange efficiency. J. Theor. Biol. (2016), http://dx.doi.org/10.1016/j.jtbi.2016.06.037

Table 3
Percentage change in oxygen uptake rate from the baseline case with variation of the model parameters.

Parameter	% change in parameter	% change in oxygen uptake rate	
		Decrease	Increase
Model Geometry			
τ	10	−58.1	6.59
ω	25	20.5	119
x_v	25	−24.6	–
d	25	−38	45.8
l_s	10	41.2	−53.1
d_s	10	−54.1	−1.83
l_d/l_p	10	–	80.0
d_d/d_p	10	−55.4	−55.5
θ_b	10	−8.65	−8.16
ϕ_{TV}	10	15.0	−11.4
d_{TV}	10	21.3	−16.6
Blood flow model			
μ	10	9.75	−8.18
P_{in}	10	−9.01	8.79
P_{out}	10	1.76×10^{-4}	-1.66×10^{-4}
κ_{empty}	10	−0.16	0.012
Oxygen transport model			
D	10	2.94×10^{-4}	-2.93×10^{-4}
C_f	10	11.4	−11.4
α	10	−1.20	0.99
C_{in}	10	−21.4	21.4

Length of villous elements (l_s): Often, pathology is associated with a change in the balance of vessel branching and elongation (Kingdom and Kaufmann, 1997). While the villous tree 'fills' the placental volume, it may do so with fewer, longer branches (or conversely more, shorter branches). By changing l_s, trees with these branching properties were generated. The effect of l_s on placental oxygen uptake, the number of terminal elements in the branching tree, the amount of IVS filled with tissue (defined as the proportion of sampling grid elements containing branches or TBs), and velocity of blood emerging from the SA are shown in Fig. 3. There is a non-linear relationship between l_s and oxygen uptake rate. As l_s increases from 1.6 mm, the villous tree begins to fill more of the IVS, and so can take up more oxygen. However, as l_s continues to increase, there is a reduction in the number of villous branches that can fit into the domain, resulting in a reduction in the number of terminal villi and consequently oxygen uptake. Finally, the tree becomes sparse enough that an increase in blood flow into the IVS is possible (with the same driving pressure) with maternal blood travelling more deeply into the IVS and oxygen uptake begins to increase again. An illustration of how the villous tree fills the domain, and oxygen penetration for $l_s = 2$ mm and $l_s = 3$ mm are provided as Supplementary Material (Section E.1).

Branch angle (θ_b): Fig 4 shows the effects of varying θ_b, while holding all other parameters constant, on placental oxygen uptake, the number of terminal elements in the branching tree, the amount of IVS filled with tissue, and velocity of blood emerging from the SA. Oxygen uptake rate varies non-linearly with θ_b with a peak at $\theta_b = 24°$. The peaks in oxygen uptake correspond with peaks in velocity of blood flow emerging from the spiral artery. Although there are only small variations in the number of terminal branches and the space filling properties of the trees with θ_b, the different orientations of branches give rise to different conductivity fields. Villous branches and TBs spread out more around the inlet as θ_b increases, thereby allowing maternal blood to flow more freely into the IVS under the same driving pressure, resulting in an increase in inlet flow velocity. However, at some point ($\theta_b \geq 26°$) the gaps between the tree branches become so big that highly conductive paths are formed that shunt flow directly from the SA to the DVs, bypassing the depth of villous tissue. Oxygen uptake is reduced as maternal blood tends to flow along this arteriovenous shunt without penetrating deep into the placental tissue. Orientation of the villous tree, flow streamlines and oxygen penetration for $\theta_b = 18°$, $24°$ and $26°$ are provided as Supplementary Material (Section E.2).

Number of branching generations (n_b): n_b was varied while holding all other parameters constant. With less than 11 branching generations, the tree does not cover the thickness of the term placenta, which is not physiological, and so n_b between 11 and 18 were considered. n_b has only a small effect on predicted flow velocity and oxygen delivery in the absence of concurrent changes in branch length or angle.

Random variability and asymmetry: An asymmetrical villous tree with random branching angles between 10° and 40° was generated to evaluate the influence of random variability of villous tree structure on model predictions. With introduction of asymmetry, a velocity boundary condition was applied at the spiral artery to obtain Q_{in} of 5 ml/min as pressure boundary conditions at the inlet SA and outlet DVs are non-applicable. While the predicted oxygen uptake rate is close to the baseline case (0.37 ml/min per placental subunit), the flow profile and resulting oxygen distribution (Fig. 5) differ from the baseline case and follow an asymmetrical pattern in accordance with the conductivity field generated based on properties of the villous tree.

Optimality of uptake with variation in geometric parameters: A peak in oxygen exchange is seen with branch lengths near to normal values (estimated from anatomical studies). The model predicts that for the same placenta size, a larger number of short villous branches result in high density tissue and obstruct maternal flow and fewer long branches result in unimpeded maternal blood circulation but smaller gas exchange surface. The model also predicts an optimum oxygen exchange when the branching angle is 24°, where villous branches and TBs are spread out sufficiently to channel maternal blood flow into the depth of the placental tissue for oxygen exchange without being shunted directly into the DVs. Without concurrent change in the branch length and angles, the number of branching generations has a small effect on oxygen exchange. The remaining model parameters, including the dimensions of the domain and maternal vasculature, blood flow and oxygen transport parameters, do not display peaks in predicted oxygen uptake within the physiological ranges analysed, although as shown in Table 3, some parameters show uniform increases or decreases in predicted oxygen uptake across the ranges considered.

3.4. The distribution of exchange interfaces

To better reflect the *in vivo* distribution of oxygen uptake described in the literature (Benirschke et al., 2006), the distribution of oxygen exchange surfaces was varied regionally. First, the oxygen exchange capacity (or the parameter α) was assumed to be the same at each placenta-IVS interface, but oxygen exchange was switched on and off regionally. Oxygen exchange was assumed to occur 1) evenly through the whole IVS (no influence of structure as in previous studies (Chernyavsky et al., 2010)), 2) only in terminal villi, or 3) only in stem and intermediate villi. Second, the parameter α was assumed to vary regionally according to the structural properties of villi and uptake was assumed to be 1) proportional to the average pO_2 in equally sized regions representing central and peripheral tissue, as well as basal, mid-placenta, and chorionic tissue as marked in Fig. 1a of the Supplementary Material, 2) inversely proportional to the average pO_2 in the regions, and 3) inversely proportional to the average harmonic thickness of the villous membranes (τvm) estimated by Critchley and Burton

Please cite this article as: Lin, M., et al., A multiscale model of placental oxygen exchange: The effect of villous tree structure on exchange efficiency. J. Theor. Biol. (2016), http://dx.doi.org/10.1016/j.jtbi.2016.06.037

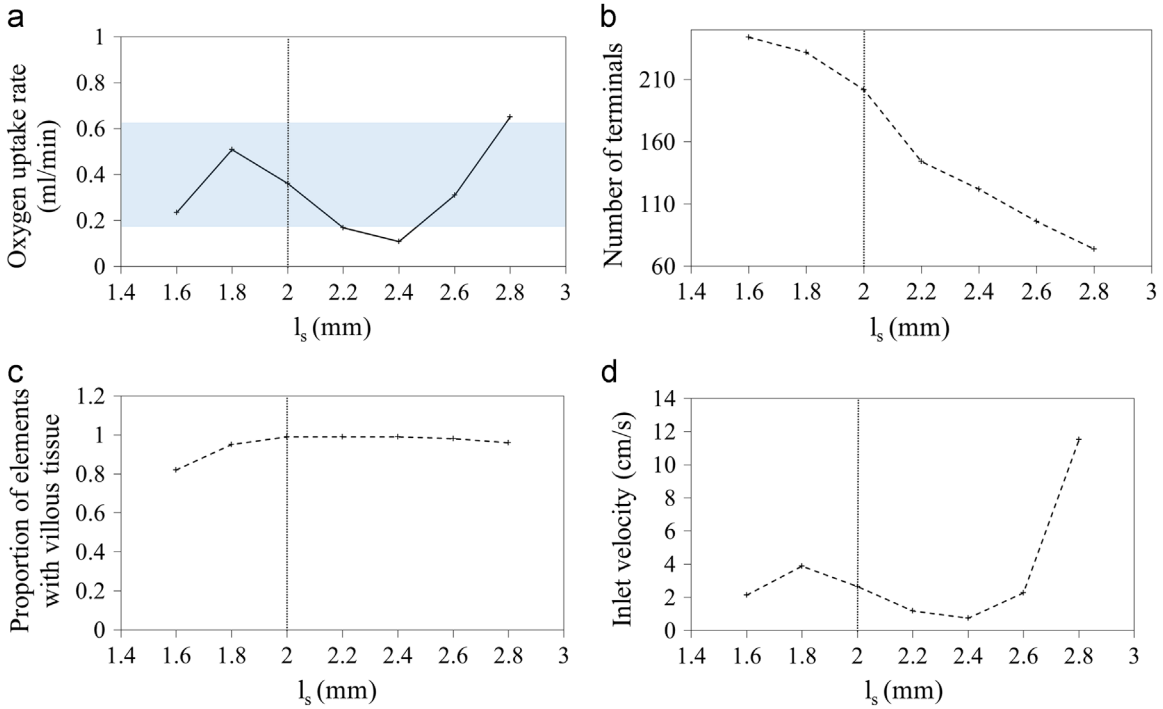

Fig. 3. The effect of the length of the stem branch (l_s) on model predictions, as all other parameters were held constant. Increasing l_s effectively increases the length of all branches in the villous tree. A range of $l_s > 1.6$ was considered, as below this range the generated tree does not fill the thickness of the term placenta. (a) Oxygen uptake rate is a non-linear function of l_s. (b) An increase in l_s gives rise to reduced number of terminal villi as the tree has fewer generations. (c) The amount of sampling grid elements containing villous tissue increases with l_s at first and then begins to slowly decrease as the tree becomes more sparse. (d) Blood flow velocity into the intervillous space is non-linear with l_s with similar changes to oxygen uptake rate.

(1987) in the regions. Model predictions for oxygen uptake over the whole placentome and average uptake per exchange interface are shown in Fig. 6.

Compared with the baseline case when oxygen exchange occurs across the whole villous tree, uptake by stem and intermediate villi alone results in a 24.5% decrease in total oxygen uptake. However, when uptake was assumed at terminal villi alone, only a 4.2% decrease is observed. In conjunction with the finding that oxygen uptake rate per exchange surface was 1.78×10^{-3} ml/min when only terminal villi acted as exchange

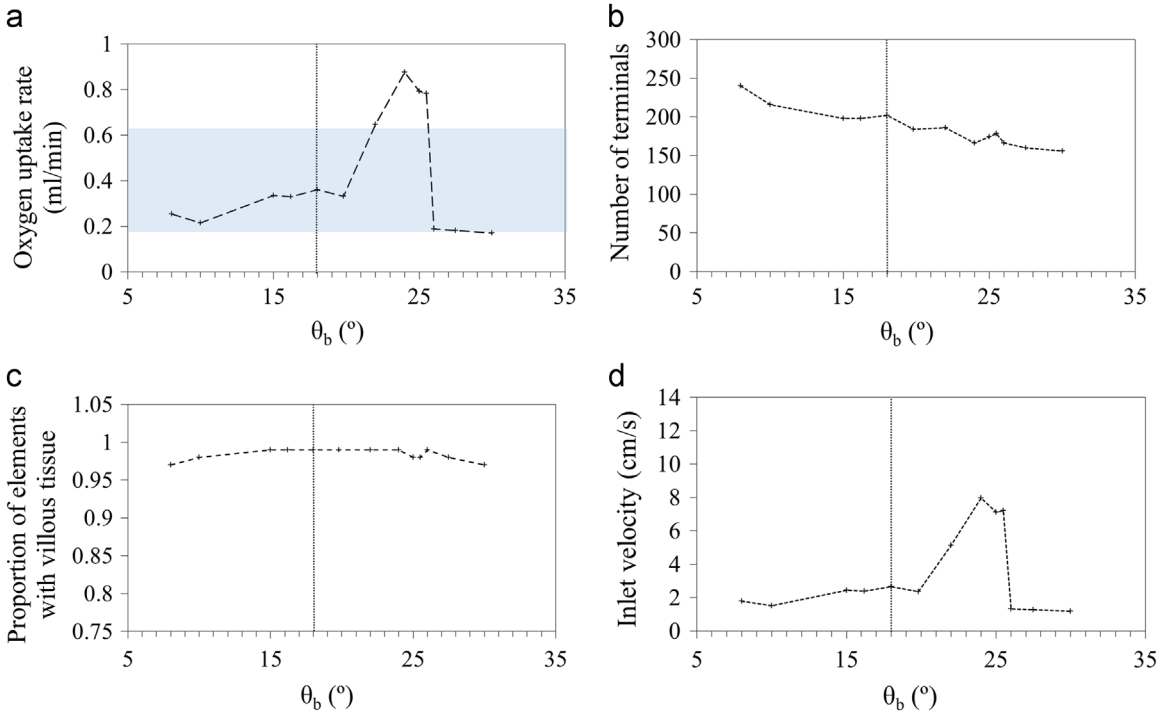

Fig. 4. The effect of branching angle (θ_b) on model predictions. (a) Oxygen uptake rate is a non-linear function of θ_b with a peak at $\theta_b = 24°$. Compared with other geometric parameters, varying θ_b results in smaller variation in (b) the number of terminal branches, and (c) the space filling properties of the generated tree. (d) Peaks in oxygen uptake correspond with peaks in blood flow velocity.

Please cite this article as: Lin, M., et al., A multiscale model of placental oxygen exchange: The effect of villous tree structure on exchange efficiency. J. Theor. Biol. (2016), http://dx.doi.org/10.1016/j.jtbi.2016.06.037

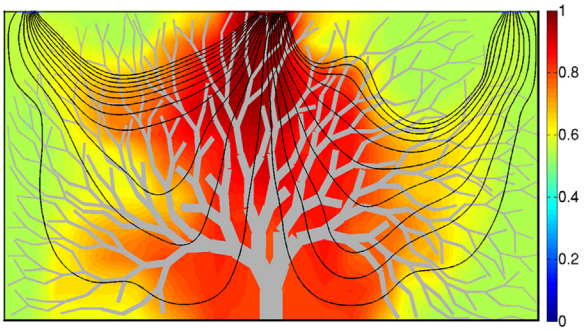

Fig. 5. Flow streamlines (black lines) and normalised oxygen concentration field (colours) predicted for a placentome containing a villous tree with random branching angles correspond with the asymmetrical branching of the villous tree.

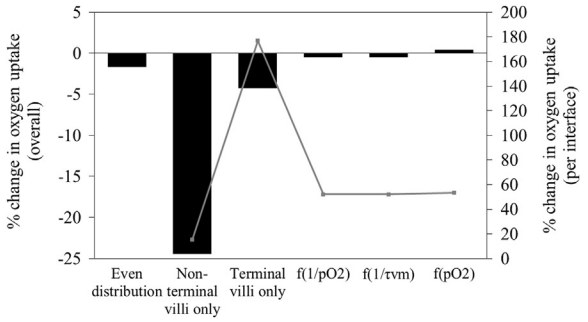

Fig. 6. Oxygen uptake with different distributions of exchange interfaces compared to the baseline case where uniform uptake occurs across the whole villous tree. Oxygen exchange at non-terminal villi only resulted in a larger decrease from the baseline case than when uptake occurs at the terminal villi only. Oxygen uptake per interface is highest when exchange occurs at the terminal villi only, suggesting that the terminal villi are the main sites for efficient oxygen exchange. A small increase in oxygen uptake from the baseline case is predicted when α is proportional to pO_2.

interfaces, our model suggests that the terminal villi of the placenta are the main sites of oxygen exchange in an efficient placenta. The model predicts an increase in oxygen uptake from the baseline case only when α is proportional to regional pO_2, or when uptake is 'easier' in high oxygen regions. This implies that a placental lobule functions more efficiently when uptake occurs in regions with high oxygen content (i.e., central regions). However, changes in uptake rate are small (less than 1%).

3.5. *Diffusive and advective transport*

The spatial variation of Péclet number was estimated across the placental subunit under baseline conditions using an average pore size of 80 μm (Serov et al., 2015) as the characteristic length of the flow domain and local speed of maternal flow at each node of the oxygen transport mesh. While oxygen transport by diffusion is accounted for in all simulations through the use of the advection-diffusion equation, oxygen transport was found to be dominated by advection throughout the domain, with Peclet number less than 1 detected in the periphery of the placentome near to the chorionic plate. Oxygen exchange in this subchorial region is negligible as this region corresponds to the relatively villus-free subchorial lake and is supplied by oxygen-depleted maternal blood which has already passed through the oxygen exchange zone. Our model includes oxygen diffusion in the transport Eq. (4), which was neglected in previous porous medium models (Chernyavsky et al., 2010), and this analysis suggests that inclusion of oxygen diffusion is indeed important regionally.

4. Discussion

In this study we have presented a model of oxygen transport in a placental subunit, which incorporates key geometric features of villous tree architecture. While computational models of oxygen transport have typically focussed on the exchange dynamics at the level of the terminal villi (Hill et al., 1972, 1973), or adopted a simplified homogeneous geometry for the IVS (Chernyavsky et al., 2010; Serov et al., 2015), the current model attempts to capture the different structural characteristics of the villous tree from the stem villi to terminal villi level to provide a representative anatomically based description of how placental structures relate to their oxygen exchange function. Even though villous tree properties have been associated with different pregnancy outcomes (Mayhew et al., 2003; Krebs et al., 1996; Egbor et al., 2006; Haeussner et al., 2014), it is unclear which geometrical features of the villous tree are most important for placental function. Here, our model provides an improved approach for the identification of key anatomical features that are crucial for placental exchange. Although the model is presented here in 2D, the composite approach employed is extendable to 3D, allowing a pragmatic approach which can be extended to represent the whole placenta without excessive computation, and can be individualised to incorporate placental structures from high resolution imaging techniques (Collins et al., 2012; Haeussner et al., 2014).

Consistency with previous studies: Our model predictions compare well to whole organ measures in terms of oxygen uptake rate and the average partial pressure of oxygen in the IVS. The predicted IVS blood flow pattern resulting from structural variations of the villous tree is consistent with the 'physiological concept' proposed in cine-angiography and injection studies (Ramsey et al., 1963), whereby it was postulated that streams or 'jets' of maternal blood enter the IVS and percolate radially through the densely packed villous tree due to dissipation of flow and pressure. The oxygen distribution generated by the model results also agrees with the decreasing central to peripheral oxygen gradient observed in primates (Ramsey et al., 1963; Richart et al., 1964) and hypothesised in humans (Wigglesworth, 1969), and is also reflective of the oxygen distribution visualised in humans using BOLD MRI (Sørensen et al., 2013).

The effect of villous branches: Detailed descriptions of the branching of the villous tree between the chorionic plate and basal plate, which have been neglected in earlier placental exchange models (Chernyavsky et al., 2011, 2010; Serov et al., 2015), are incorporated in an oxygen transport model and used to reveal its significant role in placental oxygen exchange. First, the branching angle, length and diameter of the stem and intermediate villi, all influence how villous tree branches are spread out and fill the space in the placenta, thereby affecting how maternal blood flow is constrained and channelled in the IVS. With the baseline case, we demonstrated irregular flow streamlines which were shaped by the varying conductivity field as maternal blood tends to traverse regions of non-terminal villous branches with sparser TBs over regions with dense TBs. Similarly, maternal blood tends to penetrate further into the IVS when the stem and intermediate villi are longer or more spread out, while villous branches with shorter length and smaller branch angles are more closely packed and obstruct maternal blood flow. The distribution of villous tissue around the SA inlet is especially important as it determines the tissue impedance to incoming flow, which in turn affects flow velocity and the path taken by the flow in the IVS. If the villous branches become too sparse, maternal blood flow will follow the path of least resistance and flow through the gaps between the villous branches and drain directly from the SA into the DVs, without penetrating deeper into the IVS. Such arteriovenuous shunting in the IVS is disadvantageous for oxygen exchange, which

Please cite this article as: Lin, M., et al., A multiscale model of placental oxygen exchange: The effect of villous tree structure on exchange efficiency. J. Theor. Biol. (2016), http://dx.doi.org/10.1016/j.jtbi.2016.06.037

may also explain why villus-free margins between villous trees and the basal plate have never been observed or reported. Although previous models have suggested that shunts can arise when decidual veins are close to the spiral artery (Chernyavsky et al., 2010) or when highly permeable regions are created by villi distortion due to high speed flow near the inlets and outlets (Erian et al., 1977), our model introduces a third mechanism whereby shunts can arise due to the branching structure of the villous tree. Second, the structure of the stem and intermediate villi determines the number of terminal villi and ultimately the surface area for oxygen exchange. Since the model predicts that the terminal villi are the main sites of uptake, oxygen uptake efficiency generally increases with the number of terminals.

By changing terminal villus density alone, our model predicts an optimal oxygen uptake when the total villous tissue fraction is 0.24, which is slightly lower than the value predicted in the previous homogeneous porous medium model of Chernyavsky et al. (2010). However, our model incorporates a branching component for the villous tree and predicts that the optimality of oxygen uptake rate is influenced significantly by the branching structure of the villous tree, and local changes in maternal blood flow profiles due to this structure. Our model, and previous porous medium models, predict lower optimal villus densities than stream-tube models, whose predictions of optimal villus density coincide with normal villus densities measured experimentally. In general, porous medium models appear to predict optimal villus density that corresponds to the total villus density in high-altitude pregnancies. Serov et al. (2015) suggest several reasons for predictions of optimality to differ between the two classes of model, including the use of first order uptake kinetics (which assumes uptake is proportional to local solute concentration) and the lack of explicit representation of the uptake surface. As our model allows for local variation in villous structure, we are able to assess the implications of local variation in uptake surface by varying α regionally, however this is only a qualitative approximation and this cannot be accounted for with the accuracy possible in a stream-tube model that can explicitly describe the exchange barrier, which could explain the lower optimal villus density predicted by the model. Ultimately, validation of oxygen (or any nutrient) transport models in terms of predictions of optimality will rely on concurrent measurements of villous structure as suggested by Serov et al. (2015), including artificial perfusion of the *ex vivo* placentas or primate studies to provide higher resolution data than is possible in *in vivo* human studies. Studies of *ex vivo* perfused placentas can provide information on gas exchange under different maternal and placental perfusion conditions and oxygen levels, potentially providing validation data for both porous medium and stream-tube models. For example, introduction of different oxygen content in *ex vivo* perfusion can be used to assess whether first order kinetics is sufficient to describe oxygen exchange. *Ex vivo* perfusion studies combined with 3D structural imaging of the same placenta can also tell us more about how total exchange efficiency relates to villous structure.

To date, all models are parameterised using villous density data from stereological analysis of 2D placental cross-sectional slides. Depending on the technique employed there may be errors in representing 3D villous structures *in vivo* including the lack of maternal and fetal blood flow, artefacts that can be introduced during the fixation process, and extrapolation to 3D. Post-partum analysis of histological villous density may overestimate the *in vivo* density (Serov et al., 2015). Currently, there is no established method to correct for these factors and to verify the *in vivo* villous density. Although 3D imaging is constantly evolving, and high throughput methods to measure villous structure in 3D would improve the quality and quantity of data, at this stage it remains arguable whether the placenta is performing at its optimal capability. Data describing the spatial distribution of blood flow and oxygen, such as MRI images, can potentially be used for validating model predictions in terms of flow and oxygen distributions and heterogeneity. Our model is qualitatively consistent with BOLD MRI distributions of oxygenation (Sørensen et al., 2013), but quantitative comparison is limited by difficulties in separating out maternal and fetal components in MRI. *In vivo* structural and functional imaging are evolving to give a more complete picture of the 3D placenta, with both MRI and 3D ultrasound potentially providing significant new insights into blood flow rates and distributions in the placenta. Combining this type of imaging with *ex vivo* data in the same placentas (e.g. perfusion studies, histology, or high resolution structural imaging), provides longer-term prospects for validation of models of the placenta such as this one that predict spatial variation of flow and oxygenation.

The effect of exchange potential: Simulations assessing the effects of exchange potential within the villous tree were conducted. When there was no distinction between terminal and stem villi in terms of exchange barrier properties, oxygen exchange was found to occur predominantly at the terminal villi, in line with the current understanding of the role played by terminal villi in oxygen exchange (Benirschke et al., 2006). When the exchange potential was varied as an inverse function of the average regional pO_2, the oxygen uptake efficiency is lower than when it was varied as a function of average regional pO_2, although predicted gains are small. This implies that oxygen is taken up more efficiently in regions with high oxygen content (i.e., central regions) and the uptake interfaces in these regions should possess small harmonic barrier thickness in order to optimise oxygen uptake. Critchley and Burton (1987) found that the mean harmonic barrier thickness is higher in the central regions as compared to the peripheral regions, showing more potential for exchange in the peripheral regions which is more akin to uptake as an inverse function of the average regional pO_2 which was predicted by the model to generate a lower uptake efficiency than the baseline case. These results differ in the presence of a central cavity where the model predicts oxygen exchange efficiency is highest when the exchange potential is varied as an inverse function of the average regional pO_2. Further studies are required to elucidate whether structural changes observed in the exchange surfaces in low oxygen regions are beneficial to the placenta in terms of exchange efficiency.

Relevance to IUGR: Although several stereological studies have reported morphological abnormalities of the villous tree in pathological conditions (Mayhew et al., 2003; Krebs et al., 1996; Egbor et al., 2006), the structure-function relationship between the abnormalities of the placental villi and oxygen uptake efficiency remains hypothetical. As it is impossible to make direct measurement of the *in vivo* placenta, this model provides a channel to assess these proposed hypotheses. With the model sensitivity to villous tree geometry, the model results support the hypothesis that maldevelopment of placental villi will adversely affect placental oxygen exchange. Placentas affected by IUGR are generally smaller in volume (Mayhew et al., 2003; Egbor et al., 2006). Stereological studies have revealed impoverished growth of the villi. While the villus diameter remains unaffected (Mayhew et al., 2003; Egbor et al., 2006), the shorter villus length (Egbor et al., 2006) gives rise to a smaller villus volume and a smaller exchange surface area (Mayhew et al., 2003; Egbor et al., 2006). The trophoblast epithelium was also found to be thicker (Mayhew et al., 2003). A smaller placental volume (decreasing τ and ω), coupled with a smaller exchange surface area and thicker trophoblast epithelium (decreasing α) is predicted to lead to a decrease in oxygen uptake. Although a decrease in villus length (l_s) would result in an increase in oxygen uptake, the study by Krebs et al. (1996) has suggested an increase in fetoplacental vascular impedance at the fetal capillary level as the capillary loops in the

Please cite this article as: Lin, M., et al., A multiscale model of placental oxygen exchange: The effect of villous tree structure on exchange efficiency. J. Theor. Biol. (2016), http://dx.doi.org/10.1016/j.jtbi.2016.06.037

IUGR cases are sparse in number, generally elongated and less coiled than normal cases. The interplay of these factors is likely to contribute to an overall drop in the oxygen uptake rate. Assuming that oxygenated maternal blood enters into the IVS at a normal rate, the decrease in oxygen uptake rate would give rise to a higher average pO_2 in the IVS than in normal pregnancies, which is consistent with hyperoxia in the IVS as suggested by Kingdom et al. in IUGR placentas (Kingdom and Kaufmann, 1997).

Model limitations: There are several studies which aim to quantify the branching properties of villous structures (Haeussner et al., 2014; Kosanke et al., 1993), and these studies are becoming increasingly quantitative allowing incorporation of branching and 3D rotation angles (Haeussner et al., 2014). Our branching villous model aims to match as closely as possible to these existing studies, in terms of measured tree properties including branch numbers and lengths. A sensitivity analysis to villous branching parameters was conducted to assess how inaccuracies or gaps in the current data may influence results. With advancements in imaging techniques, anatomical studies using high resolution images (for example micro-CT) of the maternal vasculature distribution and geometry of the villi can be incorporated in the current methodology to improve model accuracy.

In line with the 2D simplification of the 3D villous tree structure, we have modified the Kozeny-Carman formula (which is typically applied to model 3D media) to use the area fraction occupied by the villous tree instead of volume fraction to determine a spatially varying conductivity field for approximating IVS flow and oxygen transport in 2D like previous models (Erian et al., 1977; Lecarpentier et al., 2016). Extension to 3D does not require modification of the governing equations, but does require volume fraction to be used in the Kozeny-Carman formula and an extension of villous branching algorithms to 3D (Clark et al., 2015; Tawhai et al., 2000). Although a 2D model may not completely reflect the 3D villous geometry and flow dynamics in the placenta, it is sufficient for preliminary identification of parameters with major influence on placental function. Extensions of the model into 3D can be guided by the results of this study in their parameterisation. For example, as the 2D model suggests branch angle is a key contributor to function, therefore this is 'a key parameter to determine' from emerging 3D imaging technologies.

Although our model assumed that the IVS is a porous medium and approximated blood flow in the IVS using Darcy's law as in previous models, our model moved away from a uniformly porous medium and took a step further by using a sampling grid to capture the regional variation in porosity based on the structure of the villous tree. In our model, a sampling grid window of 2 mm was used to capture regional variations in porosity while satisfying the assumption that the IVS is a porous medium. This is consistent with the findings of Chernyavsky et al. (2011) who concluded that villous structure in a 2D section is considered as a homogenised or slowly varying porous medium if the sampling grid window size is bigger than 1 mm. Even though refinement of the sampling grid will affect the porosity distribution and give rise to a distribution that approaches the geometry of the villous tree, model solution may become unreliable since Darcy's law may no longer be suitable for approximating flow given that the assumption of the IVS as a porous medium loses its validity. Ideally, the villous tree should be represented with all its stem and intermediate villus branches as well as its terminal convolutes and maternal flow and oxygen transport should be simulated based on such detailed structures. However, given the complexities involved in representing the convoluted structure of terminal villi, we took a simplified approach of homogenising the 'random' structure of terminal villi into a tissue block with an isotropic conductivity. Also, with the lack of structural definition of the TBs, it is difficult to estimate how oxygen diffusivity varies with pore size between villous branches. Given that our results suggest that diffusion is a minor driver for oxygen transport which only occurs mostly in the peripheral and subchorial regions of the placentome where oxygen uptake is negligible, it is reasonable to implement a uniform oxygen diffusivity of oxygen. While it is possible to account for conductivity anisotropy and regional variation in oxygen diffusivity based on the tree geometry or even solve for Navier-Stokes flow around the villous tree as demonstrated by Lecarpentier et al. (2016), computational cost is an issue with such a complicated geometry, especially if flow is to be modelled on a whole organ level. For similar reasons, transport in the fetal circulation was ignored and simplified as a perfect oxygen sink, where oxygen transferred from the maternal blood was assumed to be carried away immediately by the fetal circulation. While this situation does not describe the physiology perfectly, it does help tease the effects of materno-placental blood out from those of feto-placental blood flow to help elucidate the contributions that the perfusion of maternal blood makes to placental function.

Like earlier model of Chernyavsky et al. (2010), we also simplified oxygen uptake with a first order uptake kinetic by assuming that the oxygen-hemoglobin dissociation curve is linear within the pO_2 range considered in the model. In future work, the uptake kinetics could be updated to reflect the non-linear oxygen-hemoglobin dissociation behavior for a more accurate representation of oxygen exchange.

The parameter α is a measure of the diffusing capacity of the placenta, with the resistance across the trophoblast epithelium accounting for majority of the total diffusing capacity (Mayhew et al., 1984). The resistance of trophoblast epithelium varies spatially even within the terminal villi region due to the presence of locally distended fetal capillaries which give rise to vasculosyncytial membrane with particularly thin exchange barrier. As this distribution of vasculosyncytial membrane was only approximated by estimating the mean harmonic barrier thickness in the different regions of the IVS, in the future the model could be adapted to incorporate specific locations of vasculosyncytial membrane to assess their influence on uptake efficiency.

5. Conclusions

We presented a placental oxygen exchange model which incorporates key geometric features of the placental villous tree. Unlike earlier models, the model captures multiple spatial scales of villous tree structure and identifies the crucial role played by villous tree geometry in efficient oxygen exchange. This modelling framework can be used and expanded upon to bridge gaps in current knowledge arising from difficulties in extrapolating animal models to the human placenta and the impossibility of performing invasive experiments on human placentas. Ultimately, with high-resolution imaging of the placenta, we expect the modelling framework to be able to predict structure function relationships in individual placenta samples while retaining computational tractability, allowing further insights into placental physiology and pathophysiology through pregnancy.

Acknowledgements

ML is supported by a University of Auckland Doctoral Scholarship. BM was supported by the CNRS PEPS InPhyniti funding program for his travel to Auckland for this collaboration. This research was partially funded by a Royal Society of New Zealand Marsden FastStart grant (13-UOA-032) and a Rutherford Discovery Fellowship (14-UOA-019).

Please cite this article as: Lin, M., et al., A multiscale model of placental oxygen exchange: The effect of villous tree structure on exchange efficiency. J. Theor. Biol. (2016), http://dx.doi.org/10.1016/j.jtbi.2016.06.037

Appendix A. Supplementary data

Supplementary data associated with this article can be found in the online version at http://dx.doi.org/10.1016/j.jtbi.2016.06.037.

References

Acharya, G., Sitras, V., 2009. Oxygen uptake of the human fetus at term. Acta Obstetricia et Gynecologica Scandinavica 88 (1), 104–109.

Bahriawati, C., Carstensen, C., 2005. Three Matlab implementations of the lowest-order Raviart-Thomas MFEM with a posteriori error control. Computational Methods in Applied Mathematics 5 (4), 333–361.

Benirschke, K., Kaufmann, P., Baergen, R., 2006. Pathology of the Human Placenta. Springer, New York, NY.

Bonds, D., Crosby, L., Cheek, T., Hägerdal, M., Gutsche, B., Gabbe, S., 1986. Estimation of human fetal-placental unit metabolic rate by application of the Bohr principle. Journal of Developmental Physiology 8 (1), 49–54.

Boyd, P., Hamilton, W., 1970. The Human Placenta, Heffer and Sons. Cambridge, UK.

Burton, G., Woods, A., Jauniaux, E., Kingdom, J., 2009. Rheological and physiological consequences of conversion of the maternal spiral arteries for uteroplacental blood flow during human pregnancy. Placenta 30 (6), 473–482.

Castellucci, M., Schepe, M., Scheffen, I., Celona, A., Kaufmann, P., 1990. The development of the human placental villous tree. Anatomy and Embryology 181 (2), 117–128.

Chernyavsky, I., Jensen, O., Leach, L., 2010. A mathematical model of intervillous blood flow in the human placentone. Placenta 31 (1), 44–52.

Chernyavsky, I., Leach, L., Dryden, I., Jensen, O., 2011. Transport in the placenta: homogenizing haemodynamics in a disordered medium. Philosophical Transactions of the Royal Society of London A: Mathematical, Physical and Engineering Sciences 369 (1954), 4162–4182.

Clark, A., Lin, M., Tawhai, M., Saghian, R., James, J., 2015. Multiscale modelling of the feto-placental vasculature. Interface focus 5 (2), 20140078.

Collins, S., Stevenson, G., Noble, J., Impey, L., 2012. Developmental changes in spiral artery blood flow in the human placenta observed with colour Doppler ultrasonography. Placenta 33 (10), 782–787.

Critchley, G., Burton, G., 1987. Intralobular variations in barrier thickness in the mature human placenta. Placenta 8, 185–194.

Croucher, A., O'Sullivan, M., 1998. Numerical methods for contaminant transport in rivers and estuaries. Computers & Fluids 27 (8), 861–878.

de Paula, C., Ruano, R., Campos, J., Zugaib, M., 2008. Placental volumes measured by 3-dimensional ultrasonography in normal pregnancies from 12 to 40 weeks gestation. Journal of Ultrasound in Medicine 27 (11), 1583–1590.

Egbor, M., Ansari, T., Morris, N., Green, C., Sibbons, P., 2006. Maternal medicine: morphometric placental villous and vascular abnormalities in early-and late-onset pre-eclampsia with and without fetal growth restriction. BJOG: An International Journal of Obstetrics & Gynaecology 113 (5), 580–589.

Erian, F., Corrsin, S., Davis, S., 1977. Maternal, placental blood flow: a model with velocity-dependent permeability. Journal of Biomechanics 10 (11), 807–814.

Goldstick, T., Ciuryla, V., Zuckerman, L., 1976. Diffusion of oxygen in plasma and blood, in: Oxygen Transport to Tissue - II, Springer, pp. 183–190.

Haeussner, E., Buehlmeyer, A., Schmitz, C., von Koch, F., Frank, H.-G. Novel 3D microscopic analysis of human placental villous trees reveals unexpected significance of branching angles. Scientific Reports 4, 2014 Article number: 6192.

Harris, J., Ramsey, E., 1966. The morphology of human uteroplacental vasculature. Contributions to Embryology 38, 43–58.

Hempstock, J., Bao, Y., Bar-Issac, M., Segaren, N., Watson, A., Charnock-Jones, D., Jauniaux, E., Burton, G., 2003. Intralobular differences in antioxidant enzyme expression and activity reflect the pattern of maternal arterial bloodflow within the human placenta. Placenta 24 (5), 517–523.

Hill, E., Power, G., Longo, L., 1972. A mathematical model of placental O_2 transfer with consideration of hemoglobin reaction rates. American Journal of Physiology-Legacy Content 222 (3), 721–729.

Hill, E., Power, G., Longo, L., 1973. A mathematical model of carbon dioxide transfer in the placenta and its interaction with oxygen. American Journal of Physiology-Legacy Content 224 (2), 283–299.

Johannigmann, J., Zahn, V., Thieme, V., 1972. Utraschalluntersuchung mit dem Vidoson. Elecktomedica 2, 1–11.

Kingdom, J., Kaufmann, P., 1997. Oxygen and placental villous development: origins of fetal hypoxia. Placenta 18 (8), 613–621.

Kosanke, G., Castellucci, M., Kaufmann, P., Mironov, V., 1993. Branching patterns of human placental villous trees: perspectives of topological analysis. Placenta 14, 591–604.

Krebs, C., Macara, L., Leiser, R., Bowman, A., Greer, I., Kingdom, J., 1996. Intrauterine growth restriction with absent end-diastolic flow velocity in the umbilical artery is associated with maldevelopment of the placental terminal villous tree. American Journal of Obstetrics and Gynecology 175 (6), 1534–1542.

Lecarpentier, E., Bhatt, M., Bertin, G., Deloison, B., Salomon, L., Deloron, P., Fournier, T., Barakat, A., Tsatsaris, V., 2016. Computational fluid dynamic simulations of maternal circulation: wall shear stress in the human placenta and its biological implications. PloS one 11 (1), e0147262.

Leiser, R., Kosanke, G., Kaufmann, P., 1991. Human placental vascularization, Soma H (ed): Placenta: Basic Research for Clinical Application. Int. Conf. on Placenta, Tokyo, 1990, 32–45.

Lyall, F., 2005. Priming and remodelling of human placental bed spiral arteries during pregnancy - a review. Placenta 26, Supplement A, Trophoblast Research, Vol. 19, S31–S36.

Mayhew, T., Joy, C., Haas, J., 1984. Structure-function correlation in the human placenta: the morphometric diffusing capacity for oxygen at full term. Journal of Anatomy 139 (Pt 4), 691.

Mayhew, T., Ohadike, C., Baker, P., Crocker, I., Mitchell, C., Ong, S., 2003. Stereological investigation of placental morphology in pregnancies complicated by pre-eclampsia with and without intrauterine growth restriction. Placenta 24 (2), 219–226.

Pretorius, D., Nelson, T., Baergen, R., Pai, E., Cantrell, C., 1998. Imaging of placental vasculature using three-dimensional ultrasound and color power Doppler: a preliminary study. Ultrasound in Obstetrics and Gynecology 12 (1), 45–49.

Quilligan, E., Vasicka, A., Aznar, R., Lipsitz, P., Moore, T., Bloor, B., 1960. Partial pressure of oxygen in the intervillous space and the umbilical vessels. American Journal of Obstetrics and Gynecology 79, 1048–1052.

Ramsey, E., Corner Jr, G., Donner, M., 1963. Serial and cineradioangiographic visualization of maternal circulation in the primate (hemochorial) placenta. American Journal of Obstetrics and Gynecology 86, 213.

Regnault, T., Galan, H., Parker, T., Anthony, R., 2002. Placental development in normal and compromised pregnancies - a review. Placenta 23, S119–S129.

Richart, R., Doyle, G., Ramsay, G., 1964. Visualization of the entire maternal placental circulation in the rhesus monkey. American Journal of Obstetrics and Gynecology 90, 334.

Sørensen, A., Peters, D., Simonsen, C., Pedersen, M., Stausbøl-Grøn, B., Christiansen, O., Lingman, G., Uldbjerg, N., 2013. Changes in human fetal oxygenation during maternal hyperoxia as estimated by BOLD MRI. Prenatal Diagnosis 33 (2), 141–145.

Schaaps, J., Tsatsaris, V., Goffin, F., Brichant, J., Delbecque, K., Tebache, M., Collignon, L., Retz, M., Foidart, J., 2005. Shunting the intervillous space: new concepts in human uteroplacental vascularization. American Journal of Obstetrics and Gynecology 192 (1), 323–332.

Schmid-Schobein, H., 1988. Conceptional proposition for a specific microcirculatory problem: maternal blood flow in hemochorial multivillous placentae as percolation of a “porous medium”. Trophoblast Research 3, 17–38.

Serov, A., Salafia, C., Brownbill, P., Grebenkov, D., Filoche, M., 2015. Optimal villi density for maximal oxygen uptake in the human placenta. Journal of Theoretical Biology 364, 383–396.

Serov, A., Salafia, C., Filoche, M., Grebenkov, D., 2015. Analytical theory of oxygen transport in the human placenta. Journal of Theoretical Biology 368, 133–144.

Serov, A., Salafia, C., Grebenkov, D., Filoche, M., 2015. The role of morphology in mathematical models of placental gas exchange. Journal of Applied Physiology, jap–00543.

Tawhai, M., Pullan, A., Hunter, P., 2000. Generation of an anatomically based three-dimensional model of the conducting airways. Annals of Biomedical Engineering 28 (7), 793–802.

Wigglesworth, J., 1969. Vascular anatomy of the human placenta and its significance for placental pathology. BJOG: An International Journal of Obstetrics & Gynaecology 76 (11), 979–989.

Please cite this article as: Lin, M., et al., A multiscale model of placental oxygen exchange: The effect of villous tree structure on exchange efficiency. J. Theor. Biol. (2016), http://dx.doi.org/10.1016/j.jtbi.2016.06.037

A Generation of tree structure

A rule-based approach was implemented to generate tree structures in this model. A starting branch of length l_s and diameter d_s was positioned at (ω/2,0) so that the generated tree stems from the chorionic plate with an axis of symmetry aligned with the opening of the spiral artery. It was assumed that new branches occur only from existing branch tips. Before branching can occur, the following conditions had to be satisfied:

1) There must be sufficient space locally for a new branch to form. Specifically, a new branch cannot grow outside the boundary of the domain or into space already occupied by another branch.

2) The branching generation of the new branch is below the predefined total number of branching generation (n_b).

Given that both conditions were satisfied, the new branch will grow according to the dimensions specified by the daughter to parent branch length ratio (l_d/l_p), diameter ratio (d_d/d_p) and branching angle (θ_b).

With this algorithm, large voids between the domain boundaries and the stem would occur if the villous tree was defined with a uniform branching angle across all generations. As the placenta is densely packed with villous material, the branching angle for the first 4 generations were manipulated so that the domain space was completely filled. The branching angles used for the first 4 generations of the baseline case are shown in Table 1.

Branching generation	Angle between parent and left branch	Angle between parent and right branch
1	35°	35°
2	70°	10°
3	15°	45°
4	7°	45°
5 & above	18°	18°

Table 1: Branching angles selected for baseline case

At each bifurcation, the branch nearer to the middle of the domain was given precedence over the other branch in order to create a tree with branches that grow towards to the inlet source. The algorithm was implemented to create a tree occupying half of the domain and reflected to obtain the other half for full tree symmetry.

B Finite element formulations

The advection-diffusion equation used in the model was

$$\frac{\partial C_m}{\partial t} + U.\nabla C_m = D\nabla^2 C_m - \alpha(C_m - C_f). \tag{1}$$

With the Lagrange-Galerkin method, the time derivative of C_m is given by the Lagrangian derivative where the flow is tracked from the reference frame of a particle

$$\frac{DC_m}{Dt} = \frac{\partial C_m}{\partial t} + U.\nabla C_m \tag{2}$$

This pure advection equation was solved for an auxiliary unknown C_m^* by tracing the departure point of blood at each mesh node and assigning the concentration at the blood's departure point to the mesh node at the start of each timestep.

Substitution of the Lagrangian derivative into Equation 1 gives

$$\frac{DC_m}{Dt} = D\nabla^2 C_m - \alpha(C_m - C_f). \tag{3}$$

By discretising the Lagrangian derivative using explicit finite difference approximation and applying the Galerkin finite element method to the diffusion equation, the Lagrange-Galerkin formulation of Equation 1 is obtained

$$\int_\Omega \omega \frac{C_m^{n+1} - C_m^*}{\Delta t} = \int_\Omega \omega(D\nabla^2 C_m^* - \alpha(C_m^* - C_f))d\Omega. \tag{4}$$

where ω is a weighting function.

The weak formulation was obtained by applying the Green-Gauss theorem

$$\begin{aligned}&\textstyle\int_\Omega \omega \frac{C_m^{n+1} - C_m^*}{\Delta t} \\ &= -\textstyle\int_\Omega (D\nabla C_m^*.\nabla\omega - \alpha\left(C_m^* - C_f\right).\omega)d\Omega + \int_{\partial\Omega} D\nabla C_m^*.\mathbf{n}\ \omega d\Omega,\end{aligned}$$

where the boundary condition is prescribed in the form of diffusive flux:

$$\int_{\partial\Omega} -D\nabla C_m^*.\mathbf{n}\ \omega d\Omega. \tag{5}$$

C Determining oxygen content of blood

Oxygen entering into the intervillous space is bound to hemoglobin or dissolved in plasma of the maternal blood. For maternal blood with an oxygen partial pressure of pO_2, the concentration of oxygen dissolved in the maternal plasma (C_{plasma}) was obtained by:

$$C_{plasma} = 3 \times 10^{-5} \times pO_2 \; ml/ml \tag{6}$$

For oxygen bound to hemoglobin in the maternal blood, oxygen content carried by blood is related to the partial pressure of oxygen by the hemoglobin dissociation curve. A modified Hill equation is often used to establish the amount of hemoglobin saturation in blood:

$$logpO_2 = k_1 - k_2(pH - 7.4) + k_3 log(S/(100 - S)) \tag{7}$$

where $k_1 = 1.445$, $k_2 = 0.456$ and $k_3 = 0.371$. These constants are obtained by fitting Equation 7 to the dissociation curve derived by the mathematical model proposed by Dash et al. [1].

The oxygen content carried by hemoglobin (C_{Hb}) can then be calculated from the hemoglobin saturation and the oxygen capacity of hemoglobin in the blood. Oxygen capacity is given as the product of the amount of oxygen that can be carried by hemoglobin (1.34 ml/g) and the amount of hemoglobin in the blood (0.125 g/ml):

$$S = 100 \; C_{Hb}/O_2 \; capacity \tag{8}$$

The total concentration of oxygen carried in maternal blood, C_m, is given by the sum of oxygen dissolved in the plasma and oxygen bound to hemoglobin.

D Consistency of model predictions with previous modelling or experimental studies

The model, parameterised with nominal parameters, makes several predictions that show consistency with previous modelling or experimental studies. These results are summarised below.

D.1 Oxygen exchange rates and distributions

In the baseline case, the pressure difference between the inlet and outlets was set to 18.8 mmHg to generate an average volumetric flow of 5 ml/min at the inlet. The predicted oxygen uptake rate is 0.36 ml/min per placental subunit which is close to the mean fetal and placental oxygen consumption of 0.37 ml/min (0.18-0.63 ml/min) per subunit as measured in women undergoing elective cesarean section [2]. The average partial pressure of oxygen (pO_2) in the IVS predicted by the model is 33 mmHg, near the higher limit of the range measured in the literature [3, 4]. The ratio of venous return pO_2 to that in the IVS is different from the ratio recorded by Schaaps et al. [3] for pO_2 in the uterine vein to the IVS. That study attributed higher measured pO_2 in the uterine vein to the vascular anastomoses in the myometrium and since such anastomoses were not incorporated in the current model, the ratio of pO_2 in venous return to IVS is expected to be different and should be less than 1.

Figure 1a illustrates predicted oxygen distribution and blood flow streamlines in the IVS. Flow streamlines are consistent with experimental studies describing high flow and pressure near the SA inlets and a rapid dissipation of flow and pressure in regions comprising dense villous tissue, where blood percolates rather than streams. The model demonstrates a tendency for flow to pass through regions with higher hydraulic conductivity. To assess model predictions against studies that hypothesise a central to peripheral oxygen gradient [5, 6], the model geometry was split into equally sized regions representing central and peripheral tissue, as well as basal, mid-placenta, and chorionic tissue (Figure 1a). Figure 1b shows higher average oxygen concentrations centrally than peripherally, and decreasing concentrations as one moves from the basal to chorionic surfaces of the placenta, which is consistent with these previous experimental studies.

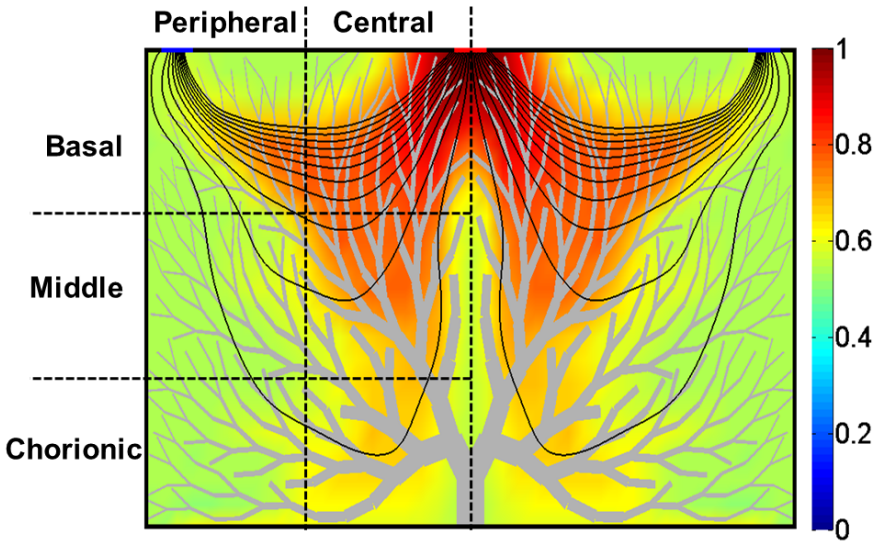

(a)

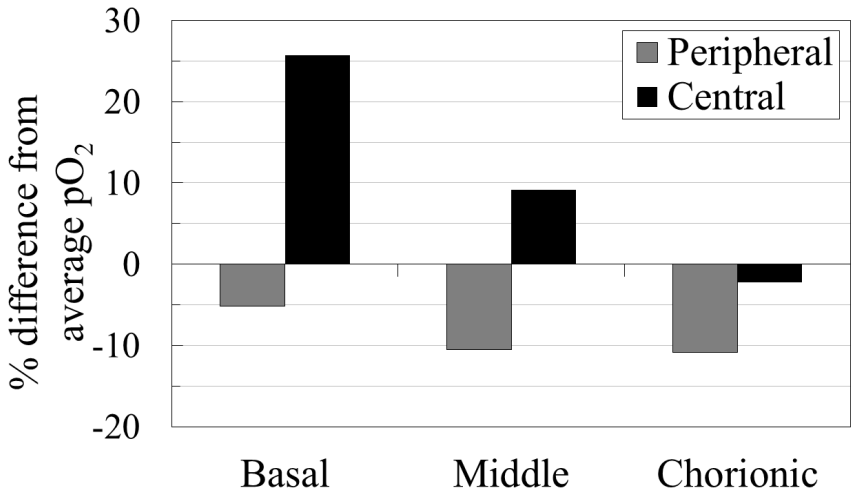

(b)

Figure 1: (a) Streamlines (black lines) and normalised oxygen concentration field (colours) predicted for a placental unit under baseline conditions. Oxygen concentration is normalised by oxygen concentration of maternal blood entering the IVS. Oxygenated maternal blood is delivered from the SA into the intervillous space which then percolates radially through the villous tissue for oxygen uptake before draining through the DVs. (b) Comparison of the average partial pressure of oxygen in the six different regions as marked in (a) demonstrated a decreasing central to peripheral oxygen concentration gradient as well as a gradient from the basal (uterine) to chorionic sides of the placenta.

D.2 Optimal villus density

Figure 2 shows the effect of varying ϕ_{TV} on the oxygen uptake capacity of the placenta. The relationship is non-linear, with low and high ϕ_{TV} displaying low efficiency (in terms of oxygen uptake) and a peak in oxygen uptake at $\phi_{TV} \approx 0.15$. In our model, the total villous area fraction incorporates both terminal villi and the villi in the tree and together this gives an optimal value for theaverage density of all villi of ≈ 0.24). This is consistent with previous porous medium models [7], our model also shows that as villous tissue becomes denser, there is an increase in the surface area available for oxygen exchange, increasing oxygen uptake. However, there is also a concurrent increase in the terminal villus impedance to maternal blood flow, and so once tissue is sufficiently dense oxygen uptake is restricted.

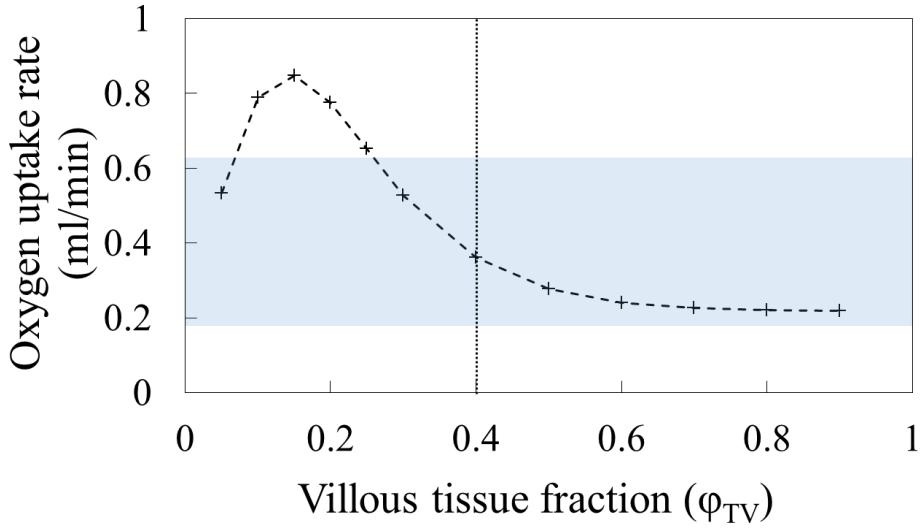

Figure 2: Predictions of oxygen uptake rate for varying terminal villous tissue density (ϕ_{TV}). The normal range of oxygen uptake rate determined from the literature is shaded. The model predicts an 'optimum' uptake rate for $\phi_{TV} \approx 0.15$, and predicts low oxygen uptake efficiency when surface area for oxygen uptake is small (at low ϕ_{TV}) or when terminal villi present a high impedance to maternal blood flow (at high ϕ_{TV}). The dotted line indicates the nominal value of ϕ_{TV}.

D.3 The effect of a central cavity

Colour Doppler ultrasonography [8] revealed 'jets' of 4 mm in width and length ranging from 3.0-8.6 mm emerging from the SAs into the IVS at 33 weeks. Assuming that jets enter the IVS in a central cavity (or a region in which the villous tree is sparse), a central cavity was introduced into the model as a relatively villus-free region having a hydraulic conductivity of κ_{empty}, which is of the same length and width of a typical jet. In the presence of a central cavity, the model predicts that oxygen rich blood is able to penetrate further and deeper into the placental tissue (Figure 3a). As in baseline predictions, a decreasing central to peripheral oxygen gradient is predicted in the presence of a central cavity. Unlike baseline predictions, when a central cavity was present, the model predicts that highest oxygen uptake occurs when α is inversely proportional to pO_2 (a 1.9% increase in uptake is predicted compared to constant uptake at all exchange interfaces) (Figure 3b). This suggests that when central cavities were present, the high uptake capacity in low oxygen regions of the placentome may be optimal. Oxygen uptake increases with cavity length to an optimal length of approximately 8 mm (Figure 3c). Small decreases in uptake occur beyond this level which may be attributed to an increased maternal blood flow velocity, which means that blood may be moving too fast for sufficient oxygen uptake to occur.

Anatomical studies have revealed the presence of a central cavity in the villous tree, typically downstream of the SA opening [5, 6]. Predicted maternal blood flow patterns are consistent with the 'physiological concepts' hypothesised by Ramsey et al. [9] and the maternal blood is clearly shown to project towards the chorionic plate due to the velocity of blood, resulting in delivery of oxygen to deeper parts of the placental tissue. The oxygen gradient between the central and peripheral regions of the placental lobule retains a decreasing gradient and is consistent with the relative antioxidant enzyme activity measured across the lobule [10]. We speculate that the 3.0-8.6 mm jets observed using colour Doppler ultrasound in near term placentas [8] are close to the optimal cavity length because longer jets do not result in increases in predicted oxygen uptake. High speed flow from SAs may mean that blood is circulated through the placenta before adequate oxygen exchange can occur and may also damage the delicate microstructure of the villi [11].

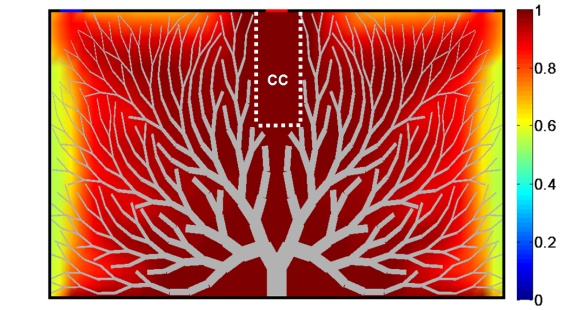

(a)

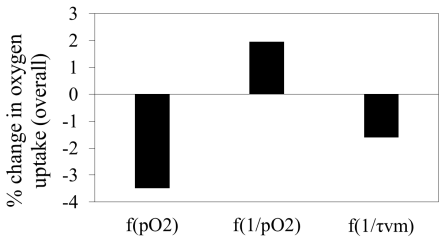

(b)

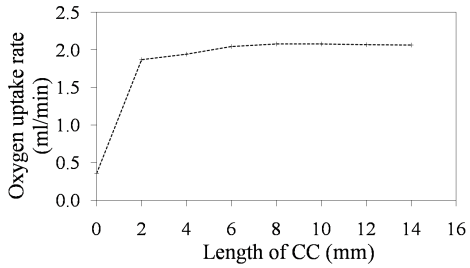

(c)

Figure 3: (a) Normalised oxygen concentration field (colours) predicted for a placental unit with a central cavity (CC) which is relatively free of villous tissue. Oxygen concentration is normalised by oxygen concentration of maternal blood entering the intervillous space. The central cavity gives rise to deeper penetration by oxygen-rich maternal blood into the placental tissue. (b) Compared to constant uptake at all exchange interfaces, the model predicts the highest oxygen uptake when α is inversely proportional to pO_2. (c) Oxygen uptake rate is predicted to increase with cavity length with the increase in distribution of oxygen-rich blood in the intervillous space. However, when the cavity length is longer than 8mm, oxygen uptake rate starts to decrease slightly.

E The relationship between geometric parameters and oxygenation

E.1 Length of villous elements (l_s):

Figure 4 illustrates how the villous tree fills the domain and oxygen distribution for $l_s = 2$ mm and $l_s = 3$ mm. The tree with $l_s = 2$ mm fills more of the IVS with more and shorter branches with a higher number of terminal villi. Although the tree with $l_s = 3$ mm is made up of fewer, longer branches and fewer terminal villi, the tree is sparse enough to result in an increase in blood flow into the IVS, which drives oxygen uptake.

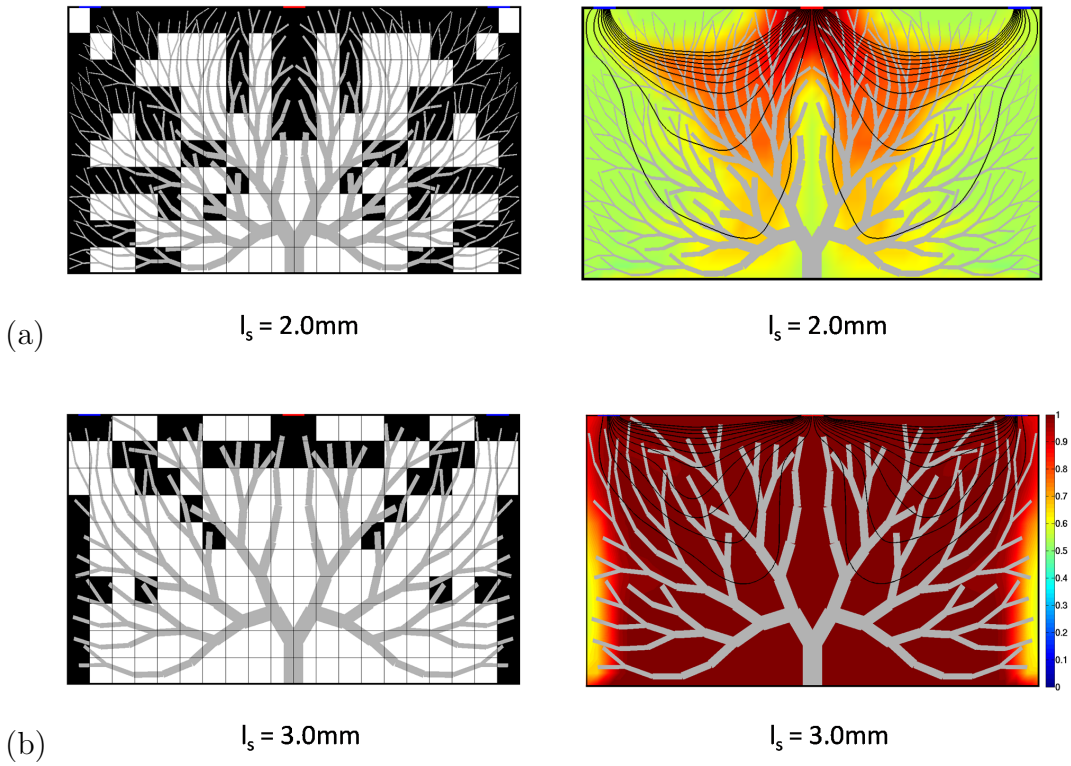

Figure 4: Space filling properties and oxygen distribution for villous tree with (a) $l_s = 2$ mm and (b) $l_s = 3$ mm. Fewer, longer villous branches and fewer terminal villi fit into the domain as l_s is increased. However, oxygen is able to penetrate further into the placental tissue as the tree becomes sparse enough at $l_s = 3$ mm for an increase in blood flow into the IVS.

E.2 Branch angle (θ_b):

Figure 5 demonstrates the space filling properties, flow streamlines and oxygen penetration around villous trees with different θ_b. Villous branches spread out more with increasing θ_b, allowing maternal blood to flow more freely and penetrate deeper into the placental tissue for oxygen exchange to occur. However, as θ_b increases further, the empty gaps between tree branches form highly conductive paths which shunt flow directly from the spiral artery to decidual veins, leading to a decrease in oxygen uptake as most of the placental tissue is bypassed.

E.3 Number of branching generations (n_b):

The effect of n_b on placental oxygen uptake, the number of terminal elements in the branching tree, the amount of IVS filled with tissue, and velocity of blood emerging from the SA are shown in Figure 6. While n_b influences the 'filling' of the placenta with tissue (as seen by increases in terminal elements and non-empty grid elements), this parameter has only a small effect on flow velocity and oxygen delivery in the absence of concurrent changes in branch length or angle. This is because the orientation of villous branches and TBs near the spiral artery inlet remain similar even as n_b is increased (Figure 7). This produces similar tissue resistance to inlet flow and hence, only small effects on inlet velocity (and oxygen uptake) is observed when n_b is varied.

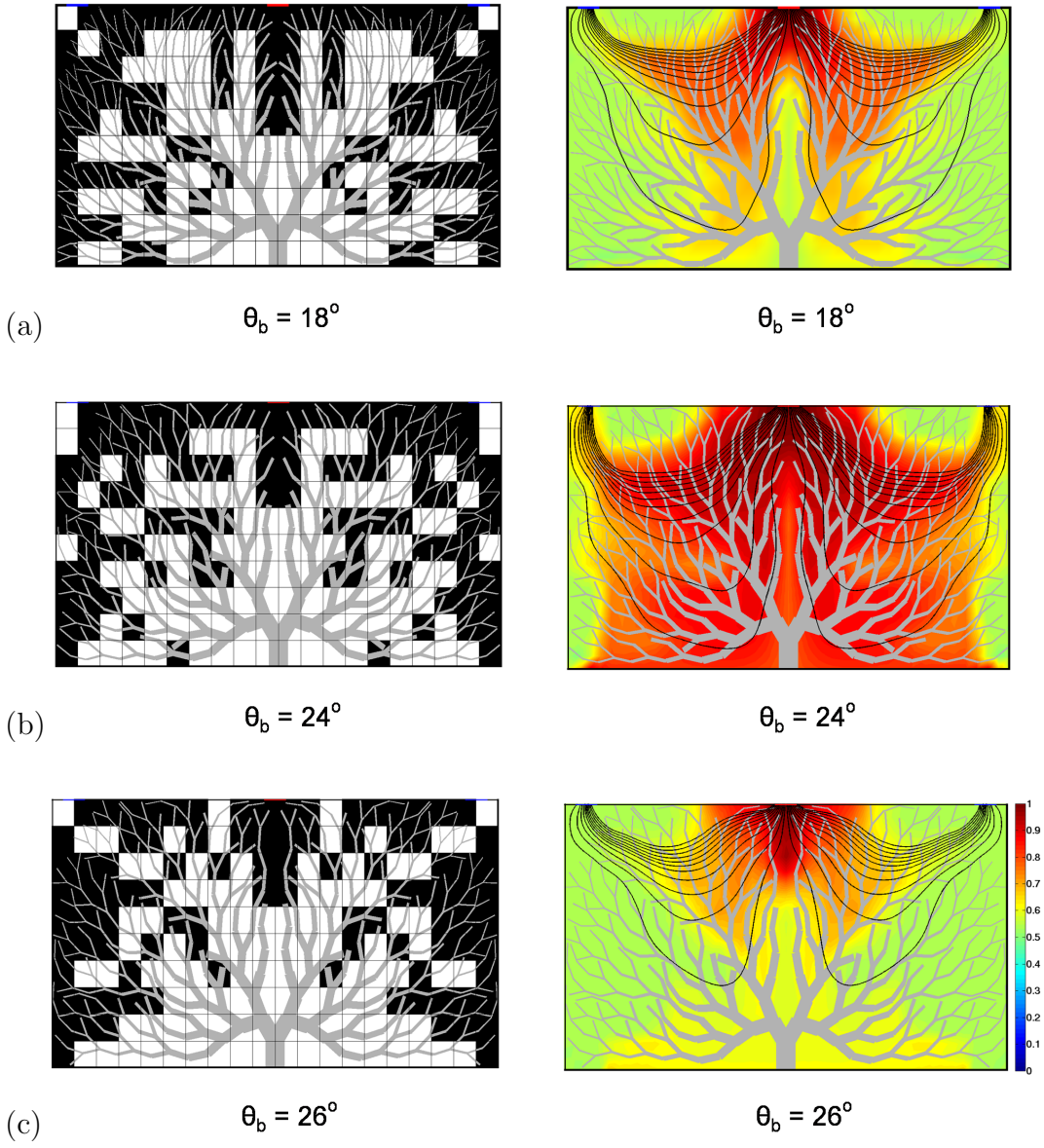

Figure 5: Space filling properties, flow streamlines and oxygen distribution for villous tree with (a) $\theta_b = 18°$, (b) $\theta_b = 24°$ and (c) $\theta_b = 26°$. Regions around the inlet becomes less filled with villous tissue with increasing θ_b. Flow penetrates deeper into the placental tissue, leading to an increase in oxygen uptake. Beyond $\theta_b = 26°$, the large spacings between branches generate paths of high hydraulic conductivity between the inlet and outlets, resulting in arteriovenous shunting.

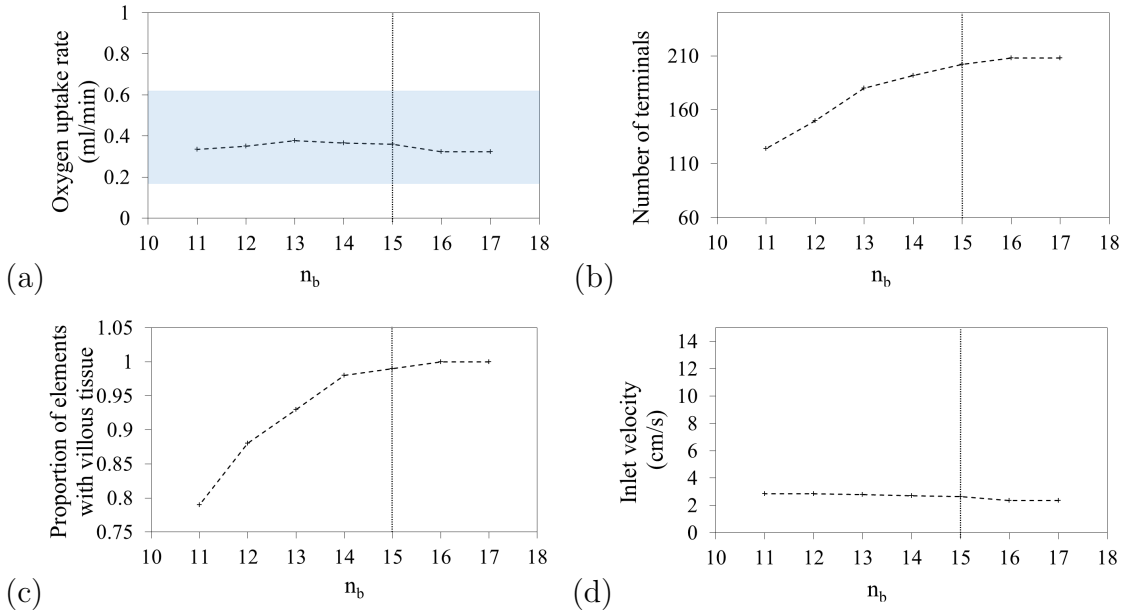

Figure 6: The effect of the number of branching generations (n_b) on model predictions. A range between 11 and 18 branching generations was considered, below this range the generated tree does not fill the thickness of the term placenta. (a) Oxygen uptake rate increases a small amount with n_b and peaks when the tree has 14 generations. (b) An increase in n_b gives rise to higher number of terminal branches in the generated villous tree. (c) The amount of sampling grid elements containing villous tissue increases with n_b. (d) Blood flow into the IVS remains almost constant.

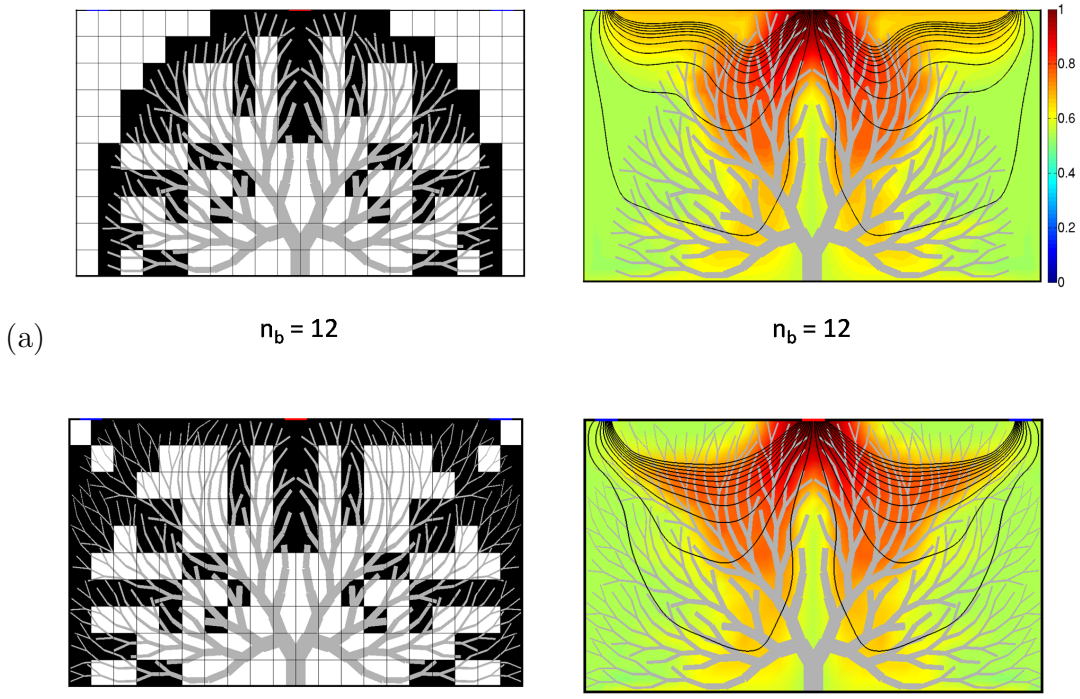

Figure 7: Space filling properties, flow streamlines, and oxygen distribution for villous tree with (a) 12 and (b) 16 branching generations. Villous branches and TBs are oriented in similar manner near the SA for both cases, providing similar resistance to inlet flow even though the streamline patterns are different.

References

[1] RK Dash and JB Bassingthwaighte. Erratum to: Blood HbO_2 and $HbCO_2$ dissociation curves at varied O_2, CO_2, pH, 2, 3-DPG and temperature levels. *Annals of Biomedical Engineering*, 38(4):1683–1701, 2010.

[2] DR Bonds, LO Crosby, TG Cheek, M Hägerdal, BB Gutsche, and SG Gabbe. Estimation of human fetal-placental unit metabolic rate by application of the Bohr principle. *Journal of Developmental Physiology*, 8(1):49–54, 1986.

[3] J Schaaps, V Tsatsaris, F Goffin, J Brichant, K Delbecque, M Tebache, L Collignon, MC Retz, and J Foidart. Shunting the intervillous space: new concepts in human uteroplacental vascularization. *American Journal of Obstetrics and Gynecology*, 192(1):323–332, 2005.

[4] EJ Quilligan, A Vasicka, R Aznar, PJ Lipsitz, T Moore, and BM Bloor. Partial pressure of oxygen in the intervillous space and the umbilical vessels. *American Journal of Obstetrics and Gynecology*, 79:1048–1052, 1960.

[5] GR Critchley and GJ Burton. Intralobular variations in barrier thickness in the mature human placenta. *Placenta*, 8:185–194, 1987.

[6] JS Wigglesworth. Vascular anatomy of the human placenta and its significance for placental pathology. *BJOG: An International Journal of Obstetrics & Gynaecology*, 76(11):979–989, 1969.

[7] IL Chernyavsky, OE Jensen, and L Leach. A mathematical model of intervillous blood flow in the human placentone. *Placenta*, 31(1):44–52, 2010.

[8] SL Collins, GN Stevenson, JA Noble, and L Impey. Developmental changes in spiral artery blood flow in the human placenta observed with colour Doppler ultrasonography. *Placenta*, 33(10):782–787, 2012.

[9] EM Ramsey, GW Corner Jr, and MW Donner. Serial and cineradioangiographic visualization of maternal circulation in the primate (hemochorial) placenta. *American Journal of Obstetrics and Gynecology*, 86: 213, 1963.

[10] J Hempstock, YP Bao, M Bar-Issac, N Segaren, AL Watson, DS Charnock-Jones, E Jauniaux, and GJ Burton. Intralobular differences in antioxidant enzyme expression and activity reflect the pattern of maternal arterial bloodflow within the human placenta. *Placenta*, 24 (5):517–523, 2003.

[11] GJ Burton, AW Woods, E Jauniaux, and JCP Kingdom. Rheological and physiological consequences of conversion of the maternal spiral arteries for uteroplacental blood flow during human pregnancy. *Placenta*, 30(6):473–482, 2009.